

Anharmonic Vibrational Analysis of Biomolecules and Solvated Molecules Using Hybrid QM/MM Computations

Kiyoshi Yagi,[†] Kenta Yamada,[†] Chigusa Kobayashi,[‡] and Yuji Sugita^{*,†,‡,§}

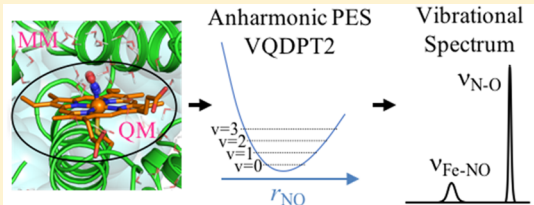
[†]Theoretical Molecular Science Laboratory, RIKEN Cluster for Pioneering Research, 2-1 Hirosawa, Wako, Saitama 351-0198, Japan

[‡]Computational Biophysics Research Team, RIKEN Center for Computational Science, 7-1-26 Minatojima-Minamimachi, Chuo-ku, Kobe, Hyogo 650-0047, Japan

[§]Laboratory for Biomolecule Function Simulation, RIKEN Center for Biosystems Dynamics Research, 1-6-5 Minatojima-Minamimachi, Chuo-ku, Kobe, Hyogo 650-0047, Japan

Supporting Information

ABSTRACT: Quantum mechanics/molecular mechanics (QM/MM) calculations are applied for anharmonic vibrational analyses of biomolecules and solvated molecules. The QM/MM method is implemented into a molecular dynamics (MD) program, GENESIS, by interfacing with external electronic structure programs. Following the geometry optimization and the harmonic normal-mode analysis based on a partial Hessian, the anharmonic potential energy surface (PES) is generated from QM/MM energies and gradients calculated at grid points. The PES is used for vibrational self-consistent field (VSCF) and post-VSCF calculations to compute the vibrational spectrum. The method is first applied to a phosphate ion in solution. With both the ion and neighboring water molecules taken as a QM region, IR spectra of representative hydration structures are calculated by the second-order vibrational quasi-degenerate perturbation theory (VQDPT2) at the level of B3LYP/cc-pVTZ and TIP3P force field. A weight-average of IR spectra over the structures reproduces the experimental spectrum with a mean absolute deviation of 16 cm⁻¹. Then, the method is applied to an enzyme, P450 nitric oxide reductase (P450nor), with the NO molecule bound to a ferric (Fe^{III}) heme. Starting from snapshot structures obtained from MD simulations of P450nor in solution, QM/MM calculations have been carried out at the level of B3LYP-D3/def2-SVP(D). The spin state of Fe^{III}(NO) is likely a closed-shell singlet state based on a ratio of N–O and Fe–NO stretching frequencies ($\nu_{\text{N-O}}$ and $\nu_{\text{Fe-NO}}$) calculated for closed- and open-shell singlet states. The calculated $\nu_{\text{N-O}}$ and $\nu_{\text{Fe-NO}}$ overestimate the experimental ones by 120 and 75 cm⁻¹, respectively. The electronic structure and solvation of Fe^{III}(NO) affect the structure around the heme of P450nor leading to an increase in $\nu_{\text{N-O}}$ and $\nu_{\text{Fe-NO}}$.



1. INTRODUCTION

Vibrational spectroscopy is one of the valuable methods to elucidate molecular mechanisms for biological functions.¹ Since molecular vibrational states are highly sensitive to intermolecular interaction, the time-resolved spectrum provides atomically detailed information on biomolecules. Advanced spectroscopic methods, such as resonance Raman,^{2,3} infrared (IR) difference,⁴ and two-dimensional IR,⁵ have further made it feasible to measure the spectrum arising from local structures of biomolecules. These techniques have been used, for example, to reveal conformational changes,^{4,6} the structure of recognition sites,^{7,8} and intermediate species in enzymatic reactions.⁹ However, extensive efforts such as mutation and isotope studies are needed to assign the observed vibrational bands and relate the spectrum with biomolecular structures. Therefore, theoretical calculations that predict the vibrational spectrum with reliable accuracy are of great importance.

Anharmonic vibrational calculations have significantly advanced in recent decades.^{10–12} Because the conventional harmonic approximation has limited accuracy, it is necessary to incorporate the anharmonicity of the potential energy surface

(PES) for quantitative purposes. The second-order vibrational perturbation theory (VPT2)^{12–14} based on a harmonic solution is widely used in conjunction with the quartic force field (QFF). Vibrational self-consistent field (VSCF)^{15,16} and post-VSCF methods,^{16–23} together with PES generation techniques using electronic structure calculations,^{24–30} have been developed as a solver of the vibrational Schrödinger equation for general polyatomic molecules. Yagi et al.^{31,32} have extended VSCF based on the quasi-degenerate perturbation theory (VQDPT), and developed a suite of programs, SINDO,³³ to generate the PES and solve the VSCF equations. Hanson-Heine et al.³⁴ have extended a partial Hessian approach^{35,36} for VPT2 calculations for large molecular systems. Bowman and co-workers^{37,38} have proposed to use normal modes localized to a water molecule, and performed vibrational configuration interaction (VCI) calculations for water clusters and ice. Methods to transform normal coordinates to local coordinates are also actively studied.^{39–47}

Received: November 27, 2018

Published: February 7, 2019

These methods are applicable to molecules with a single minimum (or a few minima) in the gas phase.

Vibrational calculations for complex systems remain a challenge, because (1) the system visits many minima with different frequencies in finite temperature, and (2) the solvent/protein environment needs to be considered. We have recently developed a weight-averaged method,^{48–50} which incorporates the former effect using classical molecular dynamics (MD) simulations and vibrational calculations based on the *ab initio* PES. In this method, MD simulations are first carried out to sample a large number of structures in the target system. Then, the trajectory is analyzed to extract relevant local structures and their statistical weights, and the vibrational calculations are carried out for each local structure to obtain its spectrum. Finally, the spectra are averaged using the weights of local structures to yield a total spectrum. The method has been used to calculate the IR and Raman spectra of a sphingomyelin bilayer^{48,51} and the IR spectrum of Nylon6 with different humidity.⁴⁹

In the present study, we combine anharmonic vibrational calculations with a quantum mechanical/molecular mechanical (QM/MM) method to incorporate the effect of solvent/protein environment on the vibrational spectrum. The QM/MM method, first proposed in seminal papers by Warshel, Levitt, and Karplus,^{52,53} is a multiscale model, which treats a local region of chemical interest by the electronic structure theory (QM) and the surrounding environment by molecular mechanics force field (MM).^{54–63} Although QM/MM has been extensively used to study enzymatic reactions, it has also been employed to compute the vibrational spectrum of biomolecules. Cui and Karplus⁶⁴ have derived an analytical Hessian for QM/MM and carried out normal-mode analyses. Tavan and co-workers^{65–68} have combined instantaneous normal-mode analyses (INMA) with QM/MM. However, these methods neglect the effect of anharmonicity. Anharmonic vibrational calculations combined with QM/MM are still scarce; the only report so far, to the best of our knowledge, is the work by Ringer and MacKerell,⁶⁹ in which VPT2 calculations have been carried out for nitrile probes in solution using QM/MM calculations. Here, we report VQDPT2 calculations based on a PES derived from QM/MM calculations.

The QM/MM method is implemented in many MD programs. The implementation in CHARMM, which was originally combined with semiempirical electronic structure methods,⁵⁵ has been extended to interface with external *ab initio* programs (CADPACK,⁷⁰ Q-Chem,⁷¹ and TURBO-MOLE⁷²) and DFTB.^{73–75} AMBER also includes the QM/MM method.^{54,76,77} Recently, a portable interface⁷⁸ has been developed and combined with FIREBALL⁷⁹ and TeraChem.⁸⁰ Other QM/MM-MD programs are also found in the literature: NAMD,^{81,82} Dynamo,^{83,84} etc. In addition, QM/MM calculations are available in electronic structure programs (Gaussian,⁸⁵ Q-Chem,⁸⁶ deMon2k,⁸⁷ Platypus,⁸⁸ etc.) and by interface programs (ChemShell⁸⁹ and PUPIL⁹⁰).

Following these works, we have implemented the QM/MM method into GENESIS^{91,92} (Generalized-Ensemble Simulation System). A QM/MM module in GENESIS interfaces QM programs (Gaussian, Q-Chem, TeraChem, and DFTB+⁹³) with MM calculations based on the CHARMM force field.⁹⁴ An efficient method to optimize the geometry, which is necessary prior to vibrational calculations, is also implemented on the basis of a limited memory version of Broyden–

Fletcher–Goldfarb–Shanno (L-BFGS-B) developed by Zhu et al.^{95–97} and a macro-/microiteration scheme.⁹⁸ A partial Hessian of a local region of the system is computed by numerical differentiations to obtain normal coordinates. Then, the anharmonic PES is generated in terms of the normal coordinates by combining GENESIS with SINDO, which is then used for solving the VSCF equations to obtain the spectrum.

We first describe an overview of the QM/MM method in Section 2, and the vibrational analysis based on the QM/MM potential in Section 3. Pilot applications are carried out for a phosphate ion in solution and P450 nitric oxide reductase (P450nor). The computational details and the results are given in Sections 4 and 5, respectively. Concluding remarks and outlooks are given in Section 6.

2. OVERVIEW OF THE QM/MM METHOD

2.1. QM/MM Potential. The QM/MM method divides a system into a QM region of particular interest and an MM region that provides its surrounding environment. The nuclei and electrons are considered explicitly in the QM region, while the MM region is described in terms of atoms defined in a molecular force field. The electrons are treated quantum mechanically by solving the following Schrödinger equation in atomic units

$$\hat{H}_e = -\frac{1}{2} \sum_i \nabla_i^2 + \sum_{i>j} \frac{1}{r_{ij}} - \sum_{i,a} \frac{Z_a}{r_{ia}} - \sum_{i,m} \frac{q_m}{r_{im}} \quad (1)$$

$$\hat{H}_e |\Psi_e\rangle = E_e |\Psi_e\rangle \quad (2)$$

where i , a , and m are indices for electrons, nuclei, and MM atoms, respectively, and Z_a and q_m are the charge of nuclei and MM atoms, respectively. r_{XY} denotes a distance between X and Y . Note that $|\Psi_e\rangle$ and E_e are the functions of coordinates of nuclei (\mathbf{R}_a) and MM atoms (\mathbf{R}_m)

$$|\Psi_e\rangle = |\Psi_e(\mathbf{r}_i; \mathbf{R}_a, \mathbf{R}_m)\rangle \quad (3)$$

$$E_e = E_e(\mathbf{R}_a, \mathbf{R}_m) \quad (4)$$

Then, the potential energy of the system is written as

$$V(\mathbf{R}_a, \mathbf{R}_m) = V^{\text{QM}}(\mathbf{R}_a, \mathbf{R}_m) + V_{\text{LJ}}^{\text{QM/MM}}(\mathbf{R}_a, \mathbf{R}_m) + V^{\text{MM}}(\mathbf{R}_m) \quad (5)$$

where V^{QM} is the QM energy defined as

$$V^{\text{QM}}(\mathbf{R}_a, \mathbf{R}_m) = E_e(\mathbf{R}_a, \mathbf{R}_m) + \sum_{a>a'} \frac{Z_a Z_{a'}}{r_{aa'}} + \sum_{a,m} \frac{Z_a q_m}{r_{am}} \quad (6)$$

and $V_{\text{LJ}}^{\text{QM/MM}}$ and V^{MM} are the Lennard-Jones interaction between nuclei and MM atoms and the classical force field for MM atoms, respectively.

$$V_{\text{LJ}}^{\text{QM/MM}}(\mathbf{R}_a, \mathbf{R}_m) = \sum_{a,m} \epsilon_{am} \left[\left(\frac{R_{am}^{\text{min}}}{r_{am}} \right)^{12} - 2 \left(\frac{R_{am}^{\text{min}}}{r_{am}} \right)^6 \right] \quad (7)$$

$$V^{\text{MM}}(\mathbf{R}_m) = V^{\text{bonded}} + \sum_{m>m'} \frac{q_m q_{m'}}{r_{mm'}} + \sum_{m>m'} \epsilon_{mm'} \left[\left(\frac{R_{mm'}^{\text{min}}}{r_{mm'}} \right)^{12} - 2 \left(\frac{R_{mm'}^{\text{min}}}{r_{mm'}} \right)^6 \right] \quad (8)$$

The derivative of the potential with respect to \mathbf{R}_a and \mathbf{R}_m gives the forces acting on nuclei and MM atoms

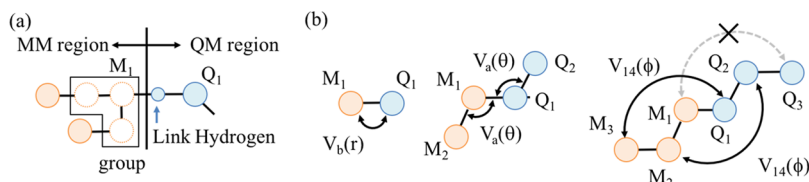


Figure 1. (a) Schematic illustration of QM and MM boundary. A hydrogen atom is added to the QM atom at the boundary (Q_1), and the MM charges are excluded in the vicinity of the link hydrogen atom (open circles). (b) Bonded terms between QM and MM atoms included in the MM potential.

$$F_a = -\frac{\partial V}{\partial \mathbf{R}_a} = -\nabla_a V^{\text{QM}} - \nabla_a V_{\text{LJ}}^{\text{QM/MM}} \quad (9)$$

$$F_m = -\frac{\partial V}{\partial \mathbf{R}_m} = -\nabla_m V^{\text{QM}} - \nabla_m V_{\text{LJ}}^{\text{QM/MM}} - \nabla_m V^{\text{MM}} \quad (10)$$

The first term in the right-hand side of eq 10 represents the electrostatic interaction between the MM charge and the electron density of the QM region, which can be rewritten in terms of the electric field, E_m ⁷⁷

$$-\nabla_m V^{\text{QM}} = q_m \left[-\langle \Psi_e | \sum_i \frac{\mathbf{r}_{im}}{r_{im}^3} | \Psi_e \rangle + \sum_a Z_a \frac{\mathbf{r}_{am}}{r_{am}^3} \right] \equiv q_m \mathbf{E}_m \quad (11)$$

In eqs 5, 9, and 10, V^{QM} , $\nabla_a V^{\text{QM}}$, and E_m are calculated using an external QM program, whereas other terms are calculated by GENESIS.

2.2. Link Atom Method. Many QM/MM applications require setting QM and MM boundaries cutting covalent bonds of a molecule, in particular, when dealing with large biomolecules. For this purpose, we have implemented the link atom method.^{54,55,57} In this method, (1) the QM atom (nuclei) at the boundary (Q_1) is terminated by a hydrogen atom, and (2) MM charges in the vicinity of the boundary are excluded in QM calculations to avoid overpolarization of the electron density (see Figure 1a). There are two options to exclude the charges: one is only the charge of the MM atom at the boundary (M_1), and the other is that of a group of MM atoms that M_1 belongs to. Note that the group is defined in the CHARMM force field. The MM potential includes bonded terms between QM and MM atoms at the boundary as shown in Figure 1b. We follow the implementation in CHARMM, where all possible combinations of QM and MM atoms are included for bond (V_b) and angle (V_a) terms, whereas the interaction between $M_3 - Q_1$ and $M_2 - Q_2$ is included, but that between $M_1 - Q_3$ is not for 4-site terms (V_{14}) such as dihedral, improper, and (ϕ , ψ) grid-based energy correction map (CMAP) terms.

In the presence of link hydrogen atoms, the QM energy becomes a function of their coordinates, \mathbf{R}_L

$$V^{\text{QM}} = V^{\text{QM}}(\mathbf{R}_a, \mathbf{R}_m, \mathbf{R}_L) \quad (12)$$

To remove the dependency on the position of link atoms, we introduce constraint to the position of the hydrogen atom.^{57,76,99} Let us place the hydrogen atom along a bond between Q_1 and M_1 with a distance d from Q_1

$$\mathbf{R}^L = \mathbf{R}^Q + \frac{d(\mathbf{R}^M - \mathbf{R}^Q)}{r_1} \quad (13)$$

where $\mathbf{R}^Q = (R_x^Q, R_y^Q, R_z^Q)$ and $\mathbf{R}^M = (R_x^M, R_y^M, R_z^M)$ are the position of Q_1 and M_1 , respectively, and r_1 is a distance

between Q_1 and M_1 . Then, the gradient of the QM energy is obtained by a chain rule

$$\frac{dV^{\text{QM}}}{dR_i^X} = \frac{\partial V^{\text{QM}}}{\partial R_i^X} + \sum_{j=x,y,z} \frac{\partial V^{\text{QM}}}{\partial R_j^L} \frac{\partial R_j^L}{\partial R_i^X} \quad (14)$$

where X is either Q or M. From eq 14, the gradient at Q_1 and M_1 is obtained as

$$\begin{aligned} \frac{dV^{\text{QM}}}{dR_i^Q} &= \frac{\partial V^{\text{QM}}}{\partial R_i^Q} + \sum_{j=x,y,z} \frac{\partial V^{\text{QM}}}{\partial R_j^L} \\ &\left[\left(1 - \frac{d}{r_1}\right) \delta_{ij} + \frac{d(R_j^M - R_j^Q)(R_i^M - R_i^Q)}{r_1^3} \right] \end{aligned} \quad (15)$$

$$\frac{dV^{\text{QM}}}{dR_i^M} = \frac{\partial V^{\text{QM}}}{\partial R_i^M} + \sum_{j=x,y,z} \frac{\partial V^{\text{QM}}}{\partial R_j^L} \left[\frac{d}{r_1} \delta_{ij} - \frac{d(R_j^M - R_j^Q)(R_i^M - R_i^Q)}{r_1^3} \right] \quad (16)$$

where δ_{ij} is the Kronecker delta.

Further details on the implementation of QM/MM in GENESIS are given in Section 1 of the Supporting Information (SI).

3. VIBRATIONAL ANALYSIS BASED ON THE QM/MM POTENTIAL

3.1. Geometry Optimization and Normal Coordinates of a Partial System. Let us assume that a local region of the system that yields the spectrum in question is known (denoted VIB region): for example, reactant/product species in enzymatic reactions, hydrogen bonds in a protein, and so on. Then, the QM region is taken to be the VIB region as well as some surrounding molecules to account for the nearest neighbor interaction that affects the vibrational states of the VIB region.

The geometry is first optimized for the QM region and a part of the MM region. An efficient optimizer is implemented using an L-BFGS-B code developed by Zhu et al.^{95–97} in terms of Cartesian coordinates. Furthermore, the macro-/micro-iteration scheme is implemented following Kästner et al.⁹⁸ This scheme optimizes the geometry in two loops of cycle. The outer loop (macroiteration) is the usual cycle for all atoms, whereas the inner loop (microiteration) optimizes only the MM atoms keeping the QM atoms fixed. In the microiteration, the electrostatic interaction between QM and MM atoms is approximated using charges of QM atoms, q_w as

$$V_e^{\text{QM/MM}}(\mathbf{R}_a, \mathbf{R}_m) = \langle \Psi_e | - \sum_{i,m} \frac{q_m}{r_{im}} | \Psi_e \rangle + \sum_{a,m} \frac{Z_a q_m}{r_{am}} \\ \cong \sum_{a,m} \frac{q_a q_m}{r_{am}} \quad (17)$$

Note that, in the presence of link atoms, the sum over MM atoms excludes MM atoms in the vicinity of the link hydrogen in which the charge is removed. The charges of QM atoms are derived, for example, from the electrostatic potential (ESP) obtained from QM calculations in the macroiteration.^{100,101} The scheme drastically reduces the computational cost, because the MM atoms are optimized in microiteration without requiring QM calculations. However, the approximation in eq 17 becomes less accurate as MM atoms move more. For a compensation for such deviations, the gradient of MM atoms is corrected as

$$\delta \mathbf{g}_m^0 = \left. \frac{\partial V_e^{\text{QM/MM}}}{\partial \mathbf{R}_m} \right|_{\mathbf{R}=\mathbf{R}_0} - \left. \frac{\partial V_e^{\text{ESP}}}{\partial \mathbf{R}_m} \right|_{\mathbf{R}=\mathbf{R}_0} \quad (18)$$

$$\mathbf{g}_m = \frac{\partial V_e^{\text{ESP}}}{\partial \mathbf{R}_m} + \delta \mathbf{g}_m^0 \quad (19)$$

where \mathbf{R}_0 denotes coordinates of the system in macroiteration. The correction recovers the gradient of the QM energy at $\mathbf{R} = \mathbf{R}_0$ and makes the gradient in macro- and microiterations consistent with each other.

Once the geometry optimization is converged, a partial Hessian matrix^{35,36} is computed for VIB atoms in $3N_v$ dimension, where N_v is the number of VIB atoms. The Hessian is obtained from numerical differentiations as

$$h_{aa'} = \frac{\partial^2 V}{\partial x_a \partial x_{a'}} \cong \frac{g_a(+\delta_{a'}) - g_a(-\delta_{a'})}{2\delta_{a'}} \quad (20)$$

where x_a denotes $3N_v$ Cartesian components of VIB atoms, δ is a step-size of numerical differentiations, and $g_a(\pm\delta_{a'})$ is the a th component of the gradient at $(x_a \pm \delta)$. QM calculations are required at $6N_v$ points to construct the Hessian matrix, which is processed in MPI parallel. Then, the Hessian is mass-weighted and diagonalized to obtain normal coordinates (Q_i) and harmonic frequencies (ω_i)

$$\omega^2 = \mathbf{L}^\dagger (\mathbf{M}^{-1/2} \mathbf{h} \mathbf{M}^{-1/2}) \mathbf{L} \quad (21)$$

$$Q_i = \sum_{a=1}^{3N_v} L_{ai} \sqrt{m_a} (x_a - x_a^{\text{eq}}) \quad (22)$$

where m_a and x_a^{eq} are the atomic mass and coordinates at the equilibrium structure, respectively, and \mathbf{M} is a diagonal matrix with $M_{aa'} = \delta_{aa'} m_a$.

3.2. Anharmonic Vibrational Calculations. The vibrational Hamiltonian is written in terms of the normal coordinates as

$$\hat{H}_{\text{vib}} = -\frac{1}{2} \sum_{i=1}^f \frac{\partial^2}{\partial Q_i^2} + V^{(n)}(\mathbf{Q}) \quad (23)$$

where f is the number of modes, and $V^{(n)}$ is the so-called n -mode representation of the potential energy surface (n MR-PES),¹⁰² in which the PES is expanded in terms of mode coupling and truncated at the n th order

$$V^{(n)} = \sum_{i=1}^f V_i(Q_i) + \sum_{i>j} V_{ij}(Q_i, Q_j) + \dots + \sum_{i_1>i_2>\dots>i_n} V_{i_n}(Q_{i_n}) \quad (24)$$

Note that the PES is a function of coordinates of all atoms, but that the coordinates of atoms out of the VIB region (\mathbf{X}) are fixed to the equilibrium geometry

$$V^{(n)}(\mathbf{Q}) = V^{(n)}(\mathbf{Q}; \mathbf{X} = \mathbf{X}^{\text{eq}}) \quad (25)$$

In other words, the present method neglects the motion of atoms out of the VIB region.

The n MR-PES can be generated using the techniques matured in the field of vibrational calculations.^{24–26,29,30,103–105} Multiresolution PES²⁹ is a composite of grid potentials²⁷ and QFF.²⁸ QFF is written in the form of n MR as

$$V^{\text{QFF}} = \sum_{i=1}^f [c_i Q_i + c_{ii} Q_i^2 + c_{iii} Q_i^3 + c_{iiii} Q_i^4] \\ + \sum_{i>j} [c_{ij} Q_i^2 Q_j + c_{jij} Q_i Q_j^2 + c_{ijij} Q_i^2 Q_j^2] \\ + \sum_{i>j>k} [c_{ijk} Q_i Q_j Q_k + c_{ijik} Q_i^2 Q_j Q_k + c_{ijjk} Q_i Q_j^2 Q_k + c_{ijkk} Q_i Q_j Q_k^2] \\ + \sum_{i>j>k>l} c_{ijkl} Q_i Q_j Q_k Q_l \quad (26)$$

The third- and fourth-order coefficients are generated by numerical differentiations of the gradient (see Section 2 in [Supporting Information](#)). The number of grid points to compute 3MR- and 4MR-QFF accumulated over all coupling order is, respectively, given as

$$N^{3\text{MR-QFF}} = 1 + 4f + 4 \binom{f}{2} = 1 + 2f + 2f^2 \quad (27)$$

$$N^{4\text{MR-QFF}} = N^{3\text{MR-QFF}} + 8 \binom{f}{3} = 1 + \frac{14f - 6f^2 + 4f^3}{3} \quad (28)$$

The grid potential is based on the harmonic oscillator discrete variable representation (HO-DVR). The number of energy points needed for generating n MR grid potential is

$$N^{n\text{MR-grid}} = \binom{f}{n} M_g^n \quad (29)$$

where M_g is the number of grid points along each coordinate. Note that the grid potentials of the low-order coupling ($n' < n$) are generated simultaneously by setting one of the grid point to be the origin, i.e., by taking M_g to be an odd number. Although the number of grid points scales steeply with respect to n and f , it may be reduced by selecting the mode of interest such that $f < 3N_v$ and by varying the size of grid according to the strength of coupling terms.

These grid points are generated by SINDO, and the QM/MM energy and gradients at the points are calculated by GENESIS in conjunction with a QM program. The loop over grid points is parallelized by MPI. The information is used to generate the multiresolution n MR-PES; in the present study, we combine 3MR-QFF and 1MR-grid PES. The PES is subsequently used for solving the vibrational Schrödinger equation by VSCF and post-VSCF methods. Details on VSCF

and VQDPT2 methods are described in Section 3 of the Supporting Information.

4. COMPUTATIONAL DETAILS

4.1. Phosphate Ion in Solution. H_2PO_4^- was prepared in a box of water ($48.6 \times 48.6 \times 48.6 \text{ \AA}^3$) by the solvation utility in VMD.¹⁰⁶ The total number of atoms was 11 747. Then, the all-atom MD simulation was performed using spdyn of GENESIS 1.2.2. The force field parameters for H_2PO_4^- and water were, respectively, those in the previous work¹⁰⁷ and TIP3P.¹⁰⁸ Following a 1000-step minimization and an equilibration NPT run for 1.0 ns, a production NVT run was carried out for 10.0 ns. The leapfrog algorithm was used for integration with a time step of 2.0 fs. SHAKE¹⁰⁹ and SETTLE¹¹⁰ were used to constrain the bond length involving hydrogen atoms. A Langevin thermostat and barostat¹¹¹ were used to control the target temperature and pressure at 300 K and 1 atm, respectively. The long-range electrostatic interaction was calculated using the smooth particle mesh Ewald (PME) method.^{112,113} The non-bonded interaction was reduced to zero between 10 and 12 \AA employing a switching function. The neighbor list was updated every 20 fs. The trajectory was saved every 10 ps, and the resulting 1000 snapshots were used for the analysis.

The snapshots were classified in terms of the number of water molecules near H_2PO_4^- (N_{wat}). The water molecule was judged to be “near” when the oxygen atom of a water molecule was within 3.5 \AA in distance of any of the oxygen atoms of H_2PO_4^- . The number of snapshot structures (N_{ss}) for each N_{wat} is shown in Table 1 indicating a distribution of N_{wat} in the

Table 1. Number of MD Snapshots Classified in Terms of the Number of Water Molecules around H_2PO_4^-

N_{wat}^a	9	10	11	12	13	14	15	16
N_{ss}^b	21	70	194	268	264	135	39	9

^aThe number of water molecules, where the oxygen atom is within 3.5 \AA of any of the oxygen atoms of H_2PO_4^- . ^bThe number of MD snapshots classified by N_{wat} .

range 9–16. Then, one representative snapshot was selected for each class of N_{wat} by *k*-means clustering method with respect to a root-mean square deviation (RMSD) of all atoms of H_2PO_4^- . The snapshot was employed as an initial structure of the QM/MM optimization. QM/MM calculations were performed combining a development version of GENESIS/atdyn with Gaussian09.⁸⁵ The QM region was set to H_2PO_4^- and the neighboring water molecules, so that the number of QM atoms was $7 + 3N_{\text{wat}}$. DFT calculations were performed at the level of B3LYP/cc-pVTZ.^{114–116}

The geometry was optimized relaxing the atoms within 10 \AA of H_2PO_4^- and fixing the others. The optimization was performed using the macro-/microiteration scheme with the Merz–Singh–Kollman charge.^{100,101} The convergence threshold was set to 0.36 and 0.54 $\text{kcal mol}^{-1} \text{ \AA}^{-1}$ for the RMS and maximum gradient, respectively. The optimization converged after 110 cycles on average and 183 cycles in maximum.

The vibrational analysis was performed for the optimized geometry taking H_2PO_4^- as a VIB region. For the calculation of a partial Hessian, 42 points of gradients were required. After the normal-mode analysis, 3MR-QFF and 1MR-grid PES (with 11 grid points to each coordinates) were constructed in 21 normal coordinates of H_2PO_4^- . The generation of 3MR-QFF

and 1MR-grid PES required 925 points of gradients and 211 points of energies, respectively. Then, VSCF and VQDPT2 were carried out using the harmonic oscillator basis functions up to $n = 10$. The quasidegenerate space in VQDPT2 was selected using $N_{\text{gen}} = 1$ and $k = 4$. The PES generation and VQDPT2 calculations were carried out using SINDO. The dipole moment surface was constructed from 1MR-grid points and used for calculating the IR intensity. The IR spectrum was constructed by a convolution of vibrational bands constructed by Lorentz functions of 40 cm^{-1} width (see Section 4 of the Supporting Information). Finally, the IR spectra for each N_{wat} were weight-averaged using $N_{\text{ss}}/N_{\text{tot}}$ as a weight, where N_{tot} is the total number of snapshots (=1000).

4.2. P450 Nitric Oxide Reductase (P450nor). The structure was taken from a recent X-ray crystal structure¹¹⁷ (PDBID 5Y5H), which contains P450nor with a NO molecule bound to a ferric iron (Fe^{III}) and crystal water molecules. First, the missing residues of the N terminus were added using GaussView5.0.¹¹⁸ The hydrogen atoms and protons were added to the system using UCSF Chimera.¹¹⁹ His96 and Glu361 were protonated based on pK_a values at pH 6.5 estimated by PROPKA3.1.^{120,121} The CHARMM36 (c36)⁹⁴ force field was used for the protein and ions, and TIP3P for water molecules. The parameters for a heme–NO unit were set as follows: (1) By considering the unit as a ferrous heme–NO⁺, the heme was described by the c36 force field for a ferrous heme, and the atomic charges of N and O atoms were set to +1.272 e and –0.272 e , respectively. (2) Other parameters for the NO (the N–O bond function and the vdW parameters) were taken from the previous study on myoglobin.^{122,123} (3) The parameters for an Fe–NO bond function were set to $r_{\text{eq}} = 1.670 \text{ \AA}$, $k_r = 350.0 \text{ kcal mol}^{-1} \text{ \AA}^{-2}$; those for $N_{\text{por}}\text{–Fe–N}$ (N_{por} is a nitrogen atom of porphyrin) and Fe–N–O angle functions were set to $\theta_{\text{eq}} = 90.0^\circ$, $k_\theta = 100.0 \text{ kcal mol}^{-1} \text{ rad}^{-2}$, and $\theta_{\text{eq}} = 158.0^\circ$, $k_\theta = 8.0 \text{ kcal mol}^{-1} \text{ rad}^{-2}$, respectively, and those for a X–Fe–N–Y dihedral function (X and Y denote an arbitrary atom type) were set to $\delta = 0.0^\circ$, $n = 4$, $k_\phi = 0.05 \text{ kcal mol}^{-1}$.

The MD simulation was first carried out fixing heavy atoms of P450nor and crystal water molecules using NAMD 2.12.⁸¹ The energy was minimized for 5000 steps in vacuum to relax the position of hydrogen atoms. The resulting structure is referred to as XtalV. Next, a simulation box of $120 \times 113 \times 101 \text{ \AA}^3$ in size was constructed adding 38 284 water molecules, 116 Na^+ , and 110 Cl^- . Then, three simulations were carried out each for 3 ns in NVT, NPT, and NVT conditions. A Langevin thermostat and the Nosé–Hoover Langevin piston methods^{124,125} were used to control the temperature at 300 K and the pressure at 1 atm, respectively. The size of the box was relaxed to $115.2 \times 108.5 \times 97.0 \text{ \AA}^3$ after the NPT simulation. The last snapshot of these simulations is referred to as XtalW.

Then, the crystal structure (P450nor and water molecules) was gradually relaxed in a series of NVT simulations using harmonic positional restraints. The force constants, initially set to 5.0 and 2.0 $\text{kcal mol}^{-1} \text{ \AA}^{-2}$ for the backbone and the others, respectively, were reduced to zero in 9 steps for 27.0 ns (see Table S1 in the Supporting Information). Then, the system was further equilibrated for 10.0 ns without restraint, followed by a production run for 70.0 ns. The temperature was controlled at 300 K with Bussi thermostat.¹²⁶ The equilibration runs with restraint were carried out with a time step of 2.0 fs using the velocity Verlet integrator, whereas the 10 ns equilibration and the 70 ns production runs were performed

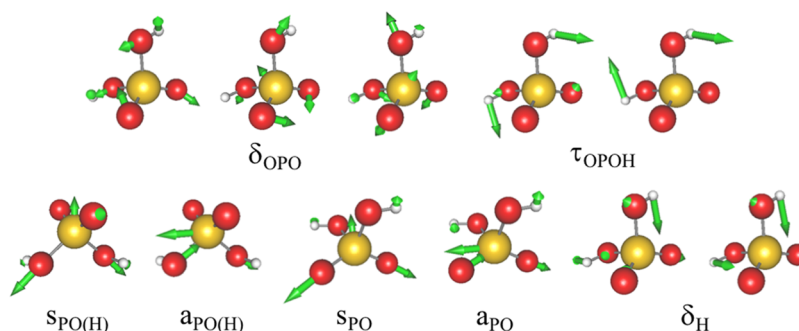


Figure 2. Vibrational modes of phosphate ion (H_2PO_4^-). δ_{OPO} , OPO bending modes; τ_{OPOH} , OPOH torsion; $s_{\text{PO(H)}}$ and $a_{\text{PO(H)}}$, symmetric and asymmetric P–OH stretching modes of hydroxyl groups; s_{PO} and a_{PO} , symmetric and asymmetric P–O stretching modes; δ_{H} , POH bending mode.

using r-RESPA integrator¹²⁷ with a time step of 2.5 fs. The long-range electrostatic interaction was calculated using the smooth PME method.^{112,113} The non-bonded interaction was reduced to zero between 10 to 12 Å using a switching function. All bonds involving hydrogen atoms were kept rigid using SHAKE¹⁰⁹ and SETTLE.¹¹⁰ These simulations were performed using spdyn of GENESIS 1.1.6. The snapshot structures of the production run were classified into five clusters using the *k*-means clustering method by fitting the structure to nitrogen atoms of the heme and measuring the RMSD of Fe, N, and O atoms. The representative structures, i.e., the center of each cluster, were found to be the snapshot at 27.27, 33.59, 35.70, 45.20, and 65.53 ns, which are referred to as NVT1, NVT2, NVT3, NVT4, and NVT5, respectively.

QM/MM calculations were performed starting from the seven snapshots, XtalV, XtalW, and NVT1–5, using a development version of GENESIS/atdyn. A QM subsystem consisted of a heme–NO unit and a side chain of Cys352 (79 atoms). The QM and MM boundary was set between C_α and C_β atoms of Cys352. The distance between a QM boundary atom and a link H atom was set to 1.0 Å. The charge of group atoms near the MM boundary was excluded in QM calculations. DFT calculations were performed at the level of BP86 or B3LYP-D3 (B3LYP hybrid functional and the D3 version of Grimme’s dispersion with Becke–Johnson damping¹²⁸) using Gaussian09, and ω B97M-V¹²⁹ using Q-Chem 4.4. The def2-SVPD¹³⁰ basis functions were used for seven atoms (four N atoms of porphyrin, a S atom of Cys352, and NO), and the def2-SVP¹³¹ basis sets for other atoms [denoted def2-SVP(D)]. The ω B97M-V calculation was also carried out using larger basis sets, def2-TZVPPD¹³⁰ for Fe, the atoms bound to Fe, and NO, and def2-TZVP¹³¹ for the others [denoted def2-TZVP(PD)]. The spin multiplicity was set to singlet. In addition to a closed-shell singlet (cs-1et) state, an open-shell singlet (os-1et) state was also calculated by a spin-unrestricted Kohn–Sham (KS) method. The initial guess orbitals for the os-1et state were prepared by combining KS orbitals obtained for the heme, the NO ligand, and the side chain of Cys352 by specifying the charge/spin multiplicity as $-1e/\text{doublet}$, $0e/\text{doublet}$, and $-1e/\text{singlet}$, respectively. An MM subsystem consisted of the remaining part of the protein and water molecules excluding the ions.

The geometry was optimized for the whole protein and water molecules within 20 Å of NO keeping the other atoms fixed. The optimization was performed using the macro/microiteration scheme based on the Merz–Singh–Kollman ESP charges^{100,101} by setting the atomic radii for Fe and H to 1.3 and 1.0 Å, respectively. A convergence threshold was set to

0.30 and 0.45 kcal mol⁻¹ Å⁻¹ for the RMS and maximum gradients, respectively. The optimization converged after 154 cycles on average and 219 cycles in maximum.

The vibrational analysis was performed setting four atoms as a VIB region; Fe, N, and O atoms of NO, and S of Cys352. For the computation of a partial Hessian, 25 points of gradients were required. After the normal-mode analysis, 3MR-QFF and 1MR-grid PES (with 11 grid points to each coordinates) were constructed for 9 normal modes excluding 3 modes related to the motion of the S atom. The generation of 3MR-QFF and 1MR-grid PES required 181 points of gradients and 91 points of energies, respectively. Then, VSCF and VQDPT2 calculations were carried out using the harmonic oscillator basis functions up to $n = 10$. The quasidegenerate space in VQDPT2 was selected using $N_{\text{gen}} = 1$ and $k = 4$. The PES generation and the VQDPT2 calculations were carried out using SINDO.

QM cluster calculations without the MM environment were also carried out for reference. The geometry of the QM subsystem was taken from the X-ray crystal structure. The position of C_β atom of Cys352 and a dihedral angle, C_β –S–Fe– N_A (N_A is one of the nitrogen atoms of a heme group), were frozen during the geometry optimization to avoid rotation of a heme plane around an Fe–S axis. The geometry optimization and the vibrational calculations were performed in the same way as above.

5. RESULTS

5.1. Phosphate Ion in Solution. The previous studies^{66,132} have reported a strong solvation effect in the vibrational spectrum of H_2PO_4^- in solution. Comparison of the spectrum in the gas phase and solution has shown that P–O stretching modes (s_{PO} and a_{PO} in Figure 2) are red-shifted by 50–170 cm⁻¹, whereas P–O–H bending and P–OH stretching modes (δ_{H} and $s_{\text{PO(H)}}$ / $a_{\text{PO(H)}}$, respectively, in Figure 2) are blue-shifted by 120–150 cm⁻¹. The large spectral shift arises from strong hydrogen bonds (HBs) formed between the ion and water molecules, which requires an accurate treatment by QM methods. Thus, H_2PO_4^- serves as a test case to assess the accuracy of the proposed method.

From the MD trajectory, the number of water molecules around H_2PO_4^- (N_{wat}) was found to be distributed in the range 9–16 with $N_{\text{wat}} = 12$ and 13 being the most abundant, as shown in Table 1. QM/MM optimized structures for $N_{\text{wat}} = 12$ and 13, shown in Figure 3, indicate that the PO^- bond accepts three water molecules whereas the hydroxyl group accepts one and donates to another water molecule. Thus, the current QM/MM calculation with $N_{\text{wat}} = 9$ –16 takes into account the

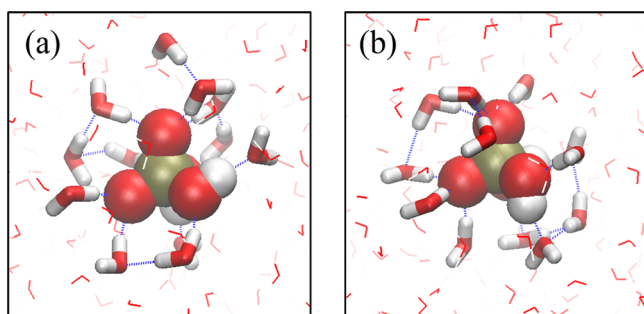


Figure 3. Optimized structures for (a) $N_{\text{wat}} = 12$ and (b) $N_{\text{wat}} = 13$. H_2PO_4^- and highlighted water molecules are QM atoms, whereas the surrounding other water molecules are MM atoms. Hydrogen bonds are indicated by blue broken lines, which are drawn when $r_{\text{OO}} < 3.2 \text{ \AA}$ and $\theta_{\text{OHO}} > 130^\circ$.

HB interaction between H_2PO_4^- and water molecules in the first solvation shell and some in the second solvation shell at the DFT level.

IR spectra obtained by the harmonic approximation for a QM/MM system with $N_{\text{wat}} = 12$ (QM/MM-12) and H_2PO_4^- in the gas phase are shown in Figure 4e and 4f, respectively. The solvation of H_2PO_4^- causes a drastic change in the spectrum as reported in the previous studies.^{66,132} The prominent peak shifts, i.e., the red-shift of ν_{PO} and ν_{PO} and

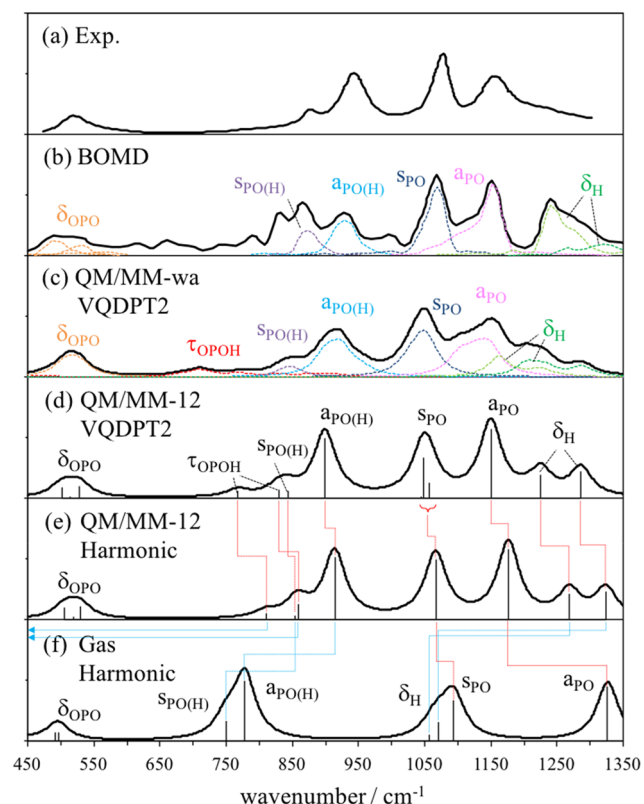


Figure 4. (a) Experimental IR spectrum of H_2PO_4^- in solution.⁶⁶ (b) IR spectrum obtained by Born–Oppenheimer (BO) MD based on the B3LYP-D/TZV2P level in the previous work.¹³² IR spectra calculated by QM/MM in this work: (c) weight-average of VQDPT2 spectra over $N_{\text{wat}} = 9–16$, (d) VQDPT2 for $N_{\text{wat}} = 12$, and (e) harmonic calculation for $N_{\text{wat}} = 12$. (f) Harmonic spectrum of H_2PO_4^- isolated in the gas phase. The spectrum is constructed using Lorentz functions with a width of 40 cm^{-1} .

the blue-shift of δ_{H} , $\nu_{\text{PO(H)}}$, and $\nu_{\text{PO(H)}}$ are clearly seen in the present result as well. Furthermore, peak positions of τ_{OPOH} are found to be dramatically shifted by more than 500 cm^{-1} . This is because the formation of HBs restricts the motion of hydroxyl groups and makes the torsional motion rigid and stiff. Such behavior is similar to bulk water, where the rotational motion of water molecules is restricted by HBs giving rise to libration bands around $400–700 \text{ cm}^{-1}$.

To further investigate the strong solvation effect, we have calculated the vibrational frequency of H_2PO_4^- using the polarizable continuum model (PCM)¹³³ and a QM/MM model which takes only H_2PO_4^- as a QM region (QM/MM-0). The results are listed in Table 2. Although PCM is capable of predicting the direction of the shift of P–O and P–OH stretching modes, the amount of shift is insufficient. Furthermore, δ_{H} and τ_{OPOH} are shifted to an opposite direction. The mean absolute deviation (MAD) is 200.5 cm^{-1} compared to QM/MM-12. In QM/MM-0, the result is significantly improved predicting the shift of δ_{H} and τ_{OPOH} in the right direction and reducing the MAD to 21.3 cm^{-1} . Nonetheless, QM/MM-0 is semiquantitative yielding a maximum deviation of 52.9 cm^{-1} for ν_{PO} . Therefore, it is essential to take not only H_2PO_4^- but also the water molecules as a QM region to account for the effect of HBs on the vibrational states of H_2PO_4^- .

Comparison of VQDPT2 and harmonic spectra in Figure 4d and 4e shows that the anharmonicity makes the frequency of all modes lower, although the overall shape of the spectrum looks similar. Nevertheless, it is notable that the size of anharmonic correction differs by the character of modes. δ_{H} and τ_{OPOH} make a larger shift than others, whereas δ_{OPO} hardly shows any shift. Thus, the scaling of harmonic frequencies by a single factor is not appropriate. It is also interesting to note that Fermi splitting is found for ν_{PO} , which is due to the resonance between a fundamental of ν_{PO} and an overtone of δ_{OPO} . The splitting makes the bandwidth slightly broader in VQDPT2 than in the harmonic spectrum.

The weight-average over $N_{\text{wat}} = 9–16$ (QM/MM-wa) smears out a peaky structure in a spectrum of QM/MM-12, as shown in Figure 4c and 4d. It is notable that the frequency of δ_{H} and τ_{OPOH} is distributed in an extremely wide range, which is a consequence of the motion of hydrogen atoms being sensitive to the hydration structure of H_2PO_4^- . Note that the broadening makes it difficult to identify the peak position of δ_{H} and τ_{OPOH} in the total spectrum. It is also interesting to see that the relative intensity of ν_{PO} and ν_{PO} is reversed in Figure 4c and 4d. Although ν_{PO} has larger intensity than ν_{PO} for each cluster, the frequency of ν_{PO} fluctuates more than that of ν_{PO} . Thus, the weight-average yields the band of ν_{PO} broader in frequency and smaller in intensity than that of ν_{PO} .

Figure 4a and 4b shows the experimental spectrum⁶⁶ and the theoretical one obtained in the previous study,¹³² respectively. The previous study carried out Born–Oppenheimer MD (BOMD) at the B3LYP-D level with TZV2P basis sets and obtained the spectrum by a Fourier transform of ensemble-averaged autocorrelation functions of the dipole moment. The two methods reproduce the experimental spectrum with similar quality, which is encouraging given that the computational techniques are totally different. One of the conclusions of the BOMD study was that the use of a nonpolarizable MM force field for water molecules (i.e., TIP3P) is inadequate for predicting the IR spectrum of H_2PO_4^- in solution. The present result is in line with this finding. We observe that treating all

Table 2. Fundamental Frequencies of H_2PO_4^- Obtained by the Harmonic Approximation and VQDPT2 for an Isolated System (Gas), PCM with Water as Solvent (PCM), a QM/MM System with and without 12 Water Molecules in the QM Region (QM/MM-12 and QM/MM-0, Respectively), and a Weight-Average over 9–16 Water Molecules (QM/MM-wa), together with the Experimental Results

mode	gas	PCM	QM/MM-0	QM/MM-12		QMMM-wa	exptl ^a
	harmonic	harmonic	harmonic	harmonic	VQDPT2	VQDPT2	
δ_{OPO}	429.8	441.5	505.9	505.6	502.5	517	521
	492.2	481.8	540.0	519.0	513.7	517	521
	497.6	492.8	552.7	529.8	527.3	517	521
τ_{OPOH}	203.5	190.1	774.6	810.5	768.0	713	
	313.3	275.1	864.7	858.5	829.3	713	
$s_{\text{PO(H)}}$	750.1	770.3	841.5	854.1	843.2	848	879
$a_{\text{PO(H)}}$	778.2	789.7	894.9	914.0	899.0	922	944
s_{PO}	1093.9	1090.4	1119.4	1066.5	1048.5	1051	1077
a_{PO}	1326.6	1275.4	1206.6	1176.5	1149.9	1145	1156
δ_{H}	1056.4	1020.3	1250.1	1268.7	1225.8	1211	1213
	1071.0	1040.3	1309.1	1324.0	1285.9	1283	

^aref 66.

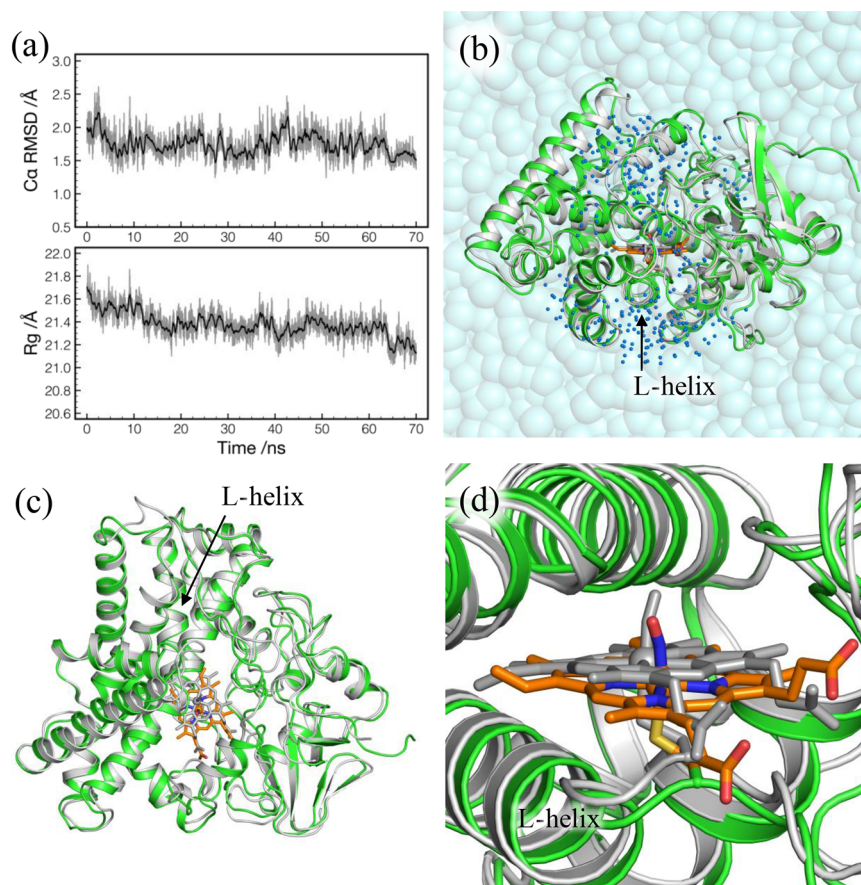


Figure 5. (a) RMSD from the X-ray crystal structure (top) and the radius of gyration (R_g) (bottom) as a function of simulation time in the production run. RMSD is calculated for C_α atoms of residues 4–403. R_g is obtained using backbone heavy atoms of residues 4–403 with mass weighting. (b) QM/MM optimized geometry of P450nor for NVT4 (colored) superimposed with the X-ray crystal structure (gray). The two structures are fit by C_α atoms of residues 4–403. Water molecules within 20 Å of NO (blue dots) are relaxed in QM/MM calculations. (c) Top view of part b without water molecules. (d) Close view of part b around the heme group with NO.

water molecules at the MM level incurs a large error in the calculated frequency (see QM/MM-0 in Table 2) and that the inclusion of water molecules in the QM region is important for quantitative purposes. Nonetheless, some improvements are worth mentioning. The previous work shows a sharp dip between a_{PO} and δ_{H} , and a prominent peak of δ_{H} , whereas the

present result shows a smooth shoulder in the range 1200–1300 cm^{-1} that resembles the experimental feature. Also, τ_{OPOH} was not identified in the previous work. These shortcomings may be due to a limited sampling time (56 ps) in the BOMD simulation. In the present study, we performed a sampling of the hydration structure for 10 ns and a clustering

Table 3. RMSD from the Crystal Structure and Geometric Parameters in the Active Site of P450nor [Bond Lengths (r in Å), Bond Angles (θ in deg), and Dihedral Angles (ϕ in deg)], and the N–O and Fe–NO Stretching Vibrations [Harmonic (ω) and VQDPT2 (ν) Frequencies Both in cm^{-1}] Obtained from QM Cluster and QM/MM Calculations Together with Experimental Values

	cs-1et ^a								os-1et ^a	exptl ^b
	Gas ^c	XtalV	XtalW	NVT1	NVT2	NVT3	NVT4	NVT5	NVT4	
C_{α} RMSD ^d		0.26	0.22	1.24	1.72	1.87	1.72	1.47	1.72	
$r_{\text{Fe-NO}}$	1.672	1.680	1.672	1.659	1.665	1.654	1.653	1.661	1.697	1.67
$r_{\text{N-O}}$	1.149	1.146	1.143	1.139	1.140	1.138	1.137	1.137	1.144	1.15
$r_{\text{Fe-S}}$	2.282	2.287	2.301	2.305	2.296	2.319	2.310	2.316	2.297	2.33
$\theta_{\text{Fe-N-O}}$	158.6	155.7	158.3	164.7	161.9	167.6	165.0	164.6	163.3	157.9
$\phi_{\text{N}_A\text{-Fe-N-O}}^e$	48.2	46.3	52.9	46.4	99.5	120.3	130.8	122.6	129.7	60.3
$\phi_{\text{C}\beta\text{-S-N-O}}$	57.3	55.7	63.3	39.3	93.0	115.0	125.3	123.3	123.8	71.4
$\omega_{\text{N-O}}$	1936.5	1946.2	1967.6	1998.1	1988.9	2008.9	2017.4	2011.6	1974.4	
$\nu_{\text{N-O}}$	1894.7	1913.4	1932.1	1966.2	1956.8	1975.4	1984.7	1981.5	1929.3	1853
$\Delta_{\text{N-O}}^f$	(41.8)	(32.8)	(35.5)	(31.9)	(32.1)	(33.5)	(32.7)	(30.1)	(45.1)	
$\omega_{\text{Fe-NO}}$	603.5	605.1	607.2	633.7	614.9	620.9	628.4	617.8	417.3	
$\nu_{\text{Fe-NO}}$	595.3	587.7	585.6	617.4	596.2	600.5	610.9	600.0	327.2	530
$\Delta_{\text{Fe-NO}}^f$	(8.2)	(17.4)	(21.6)	(16.3)	(18.7)	(20.4)	(17.5)	(17.8)	(90.1)	

^aClosed-shell singlet (cs-1et) and open-shell singlet (os-1et) states. ^bStructural parameters are from X-ray crystal structure¹¹⁷ and frequencies from resonance Raman spectra in solution.¹³⁵ ^cA QM cluster calculation in the gas phase without the MM region. ^dThe RMSD from the X-ray crystal structure calculated for C_{α} atoms of residues 4–403. ^e N_A is one of the nitrogen atoms of a heme. ^fThe difference between harmonic and VQDPT2 frequencies ($\Delta = \omega - \nu$).

in terms of N_{wat} . This procedure, albeit at the MM level, yields essential HB structures between H_2PO_4^- and water molecules that contributes to the spectrum, and leads to a smooth convergence of the spectrum with respect to the number of snapshot as small as 8 (one for each $N_{\text{wat}} = 9-16$). The result suggests that the weight-average approach⁵⁰ combining a structural sampling using MD and vibrational calculations of IR spectra using VQDPT2 and QM/MM is a promising approach to simulate the IR spectrum of solvated molecules.

5.2. P450 Nitric Oxide Reductase (P450nor). P450nor is a heme enzyme isolated from the fungus *Fusarium oxysporum* that reduces a nitric oxide (NO) to a nitrous oxide (N_2O) with electrons transferred from a nicotinamide adenine dinucleotide (NADH). The mechanism of the NO reduction has been extensively studied by spectroscopy^{117,134,135} and theoretical calculations.^{136,137} The initial step of the reaction is a binding of NO to a ferric iron (Fe^{III}) of the heme group, which is characterized by N–O and Fe–NO stretching modes.^{138–141} Here, we study these vibrations by VQDPT2 based on QM/MM.

Figure 5a plots the RMSD from the crystal structure and the radius of gyration (R_g) obtained from the MD trajectory of the production run. Both RMSD and R_g are found to be stable, suggesting that the structure of P450nor is well-maintained during the MD simulation. The RMSD is obtained as 1.74 ± 0.19 Å, and the R_g , which is 21.06 Å at the crystal structure, is slightly increased to 21.38 ± 0.12 Å.

The results of QM/MM calculations are listed in Table 3. The RMSD for XtalV and XtalW is as small as 0.26 and 0.22 Å, respectively, confirming that the optimized structures are close to the crystal structure. On the other hand, RMSD for NVT is obtained in the range 1.24–1.87 Å, indicating that the optimized structure for NVT corresponds to the one relaxed in solution. The structure of NVT4 is compared with the crystal structure in Figure 5b,c. Although NVT4 is slightly expanded in accordance with the increase in R_g , and loop regions show some deviations, the overall structure of NVT4 matches well with the crystal structure without undergoing

conformational changes or unfolding. Nevertheless, it is notable that the heme group is significantly shifted as shown in Figure 5d. The distance between Fe atoms of the crystal and NVT4 structures is 1.52 Å. A similar shift is observed for all the NVT snapshots, and thus, the shift is a general trend of P450nor in solution. Figure 5d also shows that the orientation of NO around the Fe–S axis is different between the crystal and NVT4 structures. In fact, NO is oriented in many different ways in NVT1–5, as evident from the dihedral angles, $\phi_{\text{N}_A\text{-Fe-N-O}}$ and $\phi_{\text{C}\beta\text{-S-N-O}}$, listed in Table 3. The result implies that NO rotates around the Fe–S axis in the absence of NADH.

The harmonic (ω) and VQDPT2 (ν) frequencies are also listed in Table 3. The shift in the frequency due to anharmonicity on average over the seven snapshots in the cs-1et state is found to be 32.7 ± 1.5 and 18.5 ± 1.7 cm^{-1} for the N–O and Fe–NO stretching modes, respectively. The ratio between VQDPT2 and harmonic frequencies for the N–O stretching mode, $\nu_{\text{N-O}}/\omega_{\text{N-O}}$, is obtained as 0.984, which is larger than 0.961 used in the previous study to correct the harmonic frequency.¹³⁷

Interestingly, $\nu_{\text{N-O}}$ increases as 1913.4, 1932.1, and 1956.8–1984.7 cm^{-1} for XtalV, XtalW, and NVT1–5, respectively, as the solvation is incorporated in the model. Such a drastic blue shift may be surprising given that NO is a hydrophobic molecule that does not directly interact with water molecules. The result has inspired us to carry out a QM cluster calculation without the MM environment (denoted Gas in the following), which yield 1894.7 cm^{-1} for $\nu_{\text{N-O}}$ and a similar geometry to XtalV. Figure 6 shows plots of a bond angle between Fe–N–O ($\nu_{\text{Fe-N-O}}$) and an Fe–S bond length ($r_{\text{Fe-S}}$) as a function of $\nu_{\text{N-O}}$ for Gas, XtalV, XtalW, and NVT1–5. It is notable that the increase in $\nu_{\text{N-O}}$ correlates with an expansion of $\theta_{\text{Fe-N-O}}$ and an elongation of $r_{\text{Fe-S}}$. The behavior is consistent with the so-called thiolate trans effect,¹³⁸ where the ligation of thiolate to $\text{Fe}^{\text{III}}(\text{NO})$ induces an occupation of antibonding orbitals of Fe–NO and N–O that makes Fe–NO and N–O bonds weak and an Fe–N–O angle bent (see Section 5 of the Supporting

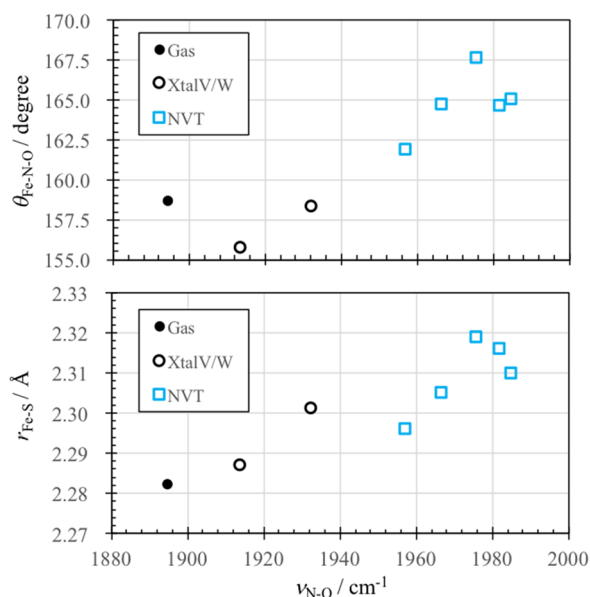


Figure 6. Fe–N–O bond angle ($\theta_{\text{Fe-N-O}}$) and the Fe–S bond length ($r_{\text{Fe-S}}$) as a function of the NO stretching frequency ($\nu_{\text{N-O}}$) calculated by QM cluster (gas) and QM/MM (XtalV, XtalW, and NVT).

Information for details). These results suggest that the solvation of P450nor elongates $r_{\text{Fe-S}}$ and weakens the thiolate trans effect, thereby inducing a strengthening of N–O bond and an increase in $\nu_{\text{N-O}}$.

$\text{Fe}^{\text{III}}(\text{NO})$ has another spin state, os-1et state, where the radical electrons of NO and Fe remain unpaired, but have an antiparallel spin so that the total system is singlet. The os-1et state is known to be close in energy to the cs-1et state.^{136,137,139} Thus, we have repeated the same calculation for the os-1et state starting from NVT4. The results are also listed in Table 3. It is notable that $\nu_{\text{N-O}}$ and $\nu_{\text{Fe-NO}}$ are both decreased in the os-1et state compared to those in the cs-1et state. This is because the radical electron of NO occupies a π^* orbital of NO and reduces the $d \rightarrow \pi^*$ back-donation, and hence, the N–O and Fe–NO bonds are both weakened. The decrease in $\nu_{\text{N-O}}$, obtained as 55.5 cm^{-1} , is consistent with the previous QM/MM calculation by Riplinger et al.¹³⁷

$\nu_{\text{N-O}}$ and $\nu_{\text{Fe-NO}}$ have been measured at 1853 and 530 cm^{-1} , respectively, by the resonance Raman spectroscopy for P450nor in solution.¹³⁵ However, the calculated $\nu_{\text{N-O}}$ and $\nu_{\text{Fe-NO}}$ for NVT1–5 in the cs-1et state, which are 1973 and

605 cm^{-1} on average, overestimate the experiment by 120 and 75 cm^{-1} , respectively. In view of such a deviation, we have extended the size of a QM region to include residues and water molecules nearby the heme group, but found that it has little effect on the frequencies (data shown in Table S2 of the Supporting Information). In the os-1et state, $\nu_{\text{N-O}}$ is decreased to 1929.2 cm^{-1} , and thus, the deviation is reduced to 76.2 cm^{-1} . However, $\nu_{\text{Fe-NO}}$ is also decreased to 327.2 cm^{-1} and deviates from the experiment by -202.8 cm^{-1} . Note that the ratio of $\nu_{\text{N-O}}/\nu_{\text{Fe-NO}}$ is obtained as 3.25 and 5.90 for the cs-1et and os-1et states, respectively. Judging from the corresponding value for the experiment (3.49), it is plausible that the spin state of $\text{Fe}^{\text{III}}(\text{NO})$ is the cs-1et state in the experimental condition.

On the basis of these findings, we have carried out QM/MM calculations with the same QM region for NVT4 in the cs-1et state using different DFT functionals and basis sets. The results are listed in Table 4. The pure functional, BP86, gives $\nu_{\text{N-O}}$ as 1881.3 cm^{-1} in agreement with the experimental value of 1853 cm^{-1} . However, $\nu_{\text{N-O}}/\nu_{\text{Fe-NO}}$ is obtained as 3.09. Furthermore, the variation in the geometry ($r_{\text{Fe-S}}$ and $\nu_{\text{Fe-N-O}}$) from B3LYP-D3 to BP86, which indicates a weakening of the thiolate trans effect, is inconsistent with the decrease in $\nu_{\text{N-O}}$. Thus, the agreement of $\nu_{\text{N-O}}$ using BP86 may be fortuitous. We also employed $\omega\text{B97M-V}$, which is one of the latest density functionals developed by Mardirossian and Head-Gordon.¹²⁹

As shown in Table 4, both $\nu_{\text{N-O}}$ and $\nu_{\text{Fe-NO}}$ are increased compared to B3LYP-D3 resulting in a larger deviation from the experiment. Nonetheless, $\nu_{\text{N-O}}/\nu_{\text{Fe-NO}}$ is obtained as 3.27 and 3.20 using the def2-SVP(D) and def2-TZVP(PD) basis sets, and the variations in the geometry and frequency are consistent with each other. Considering that cs-1et and os-1et states lie close in energy,¹³⁹ multiconfigurational methods, which can describe the two states on an equal footing, may be needed for the electronic structure calculations. Furthermore, it may be necessary to treat multiple PESs and their coupling terms in the vibrational calculation to achieve quantitative accuracy.

6. SUMMARY AND OUTLOOK

An anharmonic vibrational method based on a PES from hybrid QM/MM computations is developed for vibrational analyses of biomolecules and solvated molecules. For this purpose, we have implemented into GENESIS an interface for QM/MM calculations and methods to facilitate the normal-mode analysis: the geometry optimization (L-BFGS-B

Table 4. Representative Geometric Parameters in the Active Site of P450nor [Bond Lengths (r in \AA), Bond Angles (θ in deg)], and the N–O and Fe–NO Stretching Vibrations (ν in cm^{-1}) Obtained from QM/MM Calculations^a Using Different DFT Functionals and Basis Sets Together with Experimental Values

	BP86	B3LYP-D3	$\omega\text{B97M-V}$		exptl ^b
	def2-SVP(D) ^c	def2-SVP(D) ^c	def2-SVP(D) ^c	def2-TZVP(PD) ^d	
$r_{\text{Fe-NO}}$	1.655	1.653	1.643	1.641	1.67
$r_{\text{N-O}}$	1.160	1.137	1.121	1.115	1.15
$r_{\text{Fe-S}}$	2.337	2.310	2.298	2.300	2.33
$\theta_{\text{Fe-N-O}}$	170.0	165.0	167.5	170.0	158
$\nu_{\text{N-O}}$	1881.3	1984.7	2097.5	2054.6	1853
$\nu_{\text{Fe-NO}}$	608.0	610.9	641.1	642.0	530

^aThe snapshot is taken from NVT4, and the spin state is set to cs-1et. ^bStructural parameters are from X-ray crystal structure¹¹⁷ and frequencies from resonance Raman spectra in solution.¹³⁵ ^cdef2-SVPD for the atoms bound to Fe and NO, and def2-SVP for the others. ^ddef2-TZVPPD for Fe, the atoms bound to Fe, and NO, and def2-TZVP for the others.

minimizer and macro-/microiteration scheme) and a numerical differentiation scheme to derive a Hessian matrix for a local region. Using the resulting vibrational coordinates, multi-resolution n MR-PESs are generated from the QM/MM energy and gradient at grid points, and the PES is used for VSCF and VQDPT2 calculations to obtain the anharmonic vibrational spectrum.

The method is first applied to a phosphate ion in solution. The strong solvation effect is incorporated by treating not only the phosphate ion but also neighboring water molecules as a QM region at the B3LYP/cc-pVTZ level. The calculated spectrum demonstrates a characteristic red-shift of the P–O stretching frequency, and a blue-shift of the P–OH stretching and POH bending frequencies. The calculated band positions agree with experiment with a mean absolute deviation of 16 cm^{-1} . The present calculation also reproduces the shape of the spectrum by taking a weight-average of IR spectra over relevant hydration structures. Second, the method is applied to a NO molecule bound to a ferric (Fe^{III}) heme of P450nor. The spin state of $\text{Fe}^{\text{III}}(\text{NO})$ is suggested to be a cs -1et state based on a ratio $\nu_{\text{N-O}}/\nu_{\text{Fe-NO}}$ calculated for cs - and os -1et states. The absolute values of $\nu_{\text{N-O}}$ and $\nu_{\text{Fe-NO}}$ deviate from the experiment by $\sim 100 \text{ cm}^{-1}$, which may be due to imbalance in the QM and MM interaction or deficiency in DFT to describe the electronic structure of $\text{Fe}^{\text{III}}(\text{NO})$.

Applications of the proposed vibrational analysis method extend to a wide range. Hydrogen-bonded systems are relevant above all: for example, internal water molecules in a protein, proton transfer systems, amide modes of polypeptides and proteins, etc. To treat such systems, not only the explicit treatment of hydrogen-bonded molecules by QM calculations but also the use of advanced force fields that incorporate polarizability and charge transfer is a promising direction. These subjects will be the scope of future works.

■ ASSOCIATED CONTENT

Supporting Information

The Supporting Information is available free of charge on the ACS Publications website at DOI: 10.1021/acs.jctc.8b01193.

Implementation of QM/MM in GENESIS, QFF coefficients by numerical differentiations, VSCF and VQDPT2 methods, bandwidth of Lorentz functions, equilibration protocol of P450nor, orbital diagram of $\text{Fe}^{\text{III}}(\text{NO})$, QM/MM calculations of P450nor with extended QM region(PDF)

■ AUTHOR INFORMATION

Corresponding Author

*E-mail: sugita@riken.jp.

ORCID

Kiyoshi Yagi: 0000-0003-1120-9355

Chigusa Kobayashi: 0000-0002-5603-4619

Yuji Sugita: 0000-0001-9738-9216

Funding

This research is partially supported by the “Molecular Systems”, “iTHES”, “Integrated Lipidology”, and “Dynamic Structural Biology” projects in RIKEN (to Y. Sugita), the Center of innovation Program from Japan Science and Technology Agency, JSPS KAKENHI Grant JP26220807 and JP26119006 (to Y. Sugita), and JSPS KAKENHI Grant JP16H00857 (to K. Yagi). We used a supercomputer system,

HOKUSAI, provided by the RIKEN Information Systems Division.

Notes

The authors declare no competing financial interest.

■ ACKNOWLEDGMENTS

We thank Drs. Y. Akinaga (VINAS Co., Ltd.) and W. Mizukami (Kyushu Univ.) for their helpful comments on QM/MM methods.

■ REFERENCES

- (1) Barth, A. Infrared spectroscopy of proteins. *Biochim. Biophys. Acta, Bioenerg.* **2007**, *1767*, 1073–1101.
- (2) Mizutani, Y.; Kitagawa, T. Direct observation of cooling of heme upon photodissociation of carbonmonoxy myoglobin. *Science* **1997**, *278*, 443–446.
- (3) Fujii, N.; Mizuno, M.; Mizutani, Y. Direct Observation of Vibrational Energy Flow in Cytochrome *c*. *J. Phys. Chem. B* **2011**, *115*, 13057–13064.
- (4) Kottke, T.; Lórenz-Fonfría, V. A.; Heberle, J. The Grateful Infrared: Sequential Protein Structural Changes Resolved by Infrared Difference Spectroscopy. *J. Phys. Chem. B* **2017**, *121*, 335–350.
- (5) Ganim, Z.; Chung, H. S.; Smith, A. W.; Deflores, L. P.; Jones, K. C.; Tokmakoff, A. Amide I two-dimensional infrared Spectroscopy of proteins. *Acc. Chem. Res.* **2008**, *41*, 432–441.
- (6) Furutani, Y.; Shibata, M.; Kandori, H. Strongly hydrogen-bonded water molecules in the Schiff base region of rhodopsins. *Photochem. Photobiol. Sci.* **2005**, *4*, 661.
- (7) Johnson, P. J. M.; Koziol, K. L.; Hamm, P. Quantifying Biomolecular Recognition with Site-Specific 2D Infrared Probes. *J. Phys. Chem. Lett.* **2017**, *8*, 2280–2284.
- (8) Sekiguchi, T.; Tamura, M.; Oba, H.; Carcarbal, P.; Lozada-Garcia, R. R.; Zehnacker-Rentien, A.; Grégoire, G.; Ishiuchi, S.; Fujii, M. Molecular Recognition by a Short Partial Peptide of the Adrenergic Receptor: A Bottom-Up Approach. *Angew. Chem., Int. Ed.* **2018**, *57*, 5626–5629.
- (9) Horch, M.; Hildebrandt, P.; Zebger, I. Concepts in biomolecular spectroscopy: vibrational case studies on metalloenzymes. *Phys. Chem. Chem. Phys.* **2015**, *17*, 18222–18237.
- (10) Bowman, J. M.; Carrington, T.; Meyer, H.-D. Variational quantum approaches for computing vibrational energies of polyatomic molecules. *Mol. Phys.* **2008**, *106*, 2145–2182.
- (11) Christiansen, O. Selected new developments in vibrational structure theory: Potential construction and vibrational wave function calculations. *Phys. Chem. Chem. Phys.* **2012**, *14*, 6672–6687.
- (12) Barone, V.; Biczysko, M.; Bloino, J. Fully anharmonic IR and Raman spectra of medium-size molecular systems: accuracy and interpretation. *Phys. Chem. Chem. Phys.* **2014**, *16*, 1759–1787.
- (13) Barone, V. Anharmonic vibrational properties by a fully automated second-order perturbative approach. *J. Chem. Phys.* **2005**, *122*, No. 014108.
- (14) Bloino, J.; Biczysko, M.; Barone, V. General Perturbative Approach for Spectroscopy, Thermodynamics, and Kinetics: Methodological Background and Benchmark Studies. *J. Chem. Theory Comput.* **2012**, *8*, 1015–1036.
- (15) Bowman, J. M. Self-Consistent Field Energies and Wavefunctions for Coupled Oscillators. *J. Chem. Phys.* **1978**, *68*, 608–610.
- (16) Bowman, J. M. The Self-Consistent-Field Approach to Polyatomic Vibrations. *Acc. Chem. Res.* **1986**, *19*, 202–208.
- (17) Norris, L. S.; Ratner, M. A.; Roitberg, A. E.; Gerber, R. B. Møller-Plesset Perturbation Theory Applied to Vibrational Problems. *J. Chem. Phys.* **1996**, *105*, 11261–11267.
- (18) Christiansen, O. Vibrational Coupled Cluster Theory. *J. Chem. Phys.* **2004**, *120*, 2149–2159.
- (19) Seidler, P.; Sparta, M.; Christiansen, O. Vibrational coupled cluster response theory: A general implementation. *J. Chem. Phys.* **2011**, *134*, No. 054119.

- (20) Rauhut, G. Configuration selection as a route towards efficient vibrational configuration interaction calculations. *J. Chem. Phys.* **2007**, *127*, 184109.
- (21) Heislbeitz, S.; Rauhut, G. Vibrational multiconfiguration self-consistent field theory: Implementation and test calculations. *J. Chem. Phys.* **2010**, *132*, 124102.
- (22) Pfeiffer, F.; Rauhut, G. Multi-reference vibration correlation methods. *J. Chem. Phys.* **2014**, *140*, No. 064110.
- (23) Mizukami, W.; Tew, D. P. A second-order multi-reference perturbation method for molecular vibrations. *J. Chem. Phys.* **2013**, *139*, 194108.
- (24) Rauhut, G. Efficient calculation of potential energy surfaces for the generation of vibrational wave functions. *J. Chem. Phys.* **2004**, *121*, 9313–9322.
- (25) Kongsted, J.; Christiansen, O. Automatic generation of force fields and property surfaces for use in variational vibrational calculations of anharmonic vibrational energies and zero-point vibrational averaged properties. *J. Chem. Phys.* **2006**, *125*, 124108.
- (26) Toffoli, D.; Kongsted, J.; Christiansen, O. Automatic generation of potential energy and property surfaces of polyatomic molecules in normal coordinates. *J. Chem. Phys.* **2007**, *127*, 204106.
- (27) Yagi, K.; Taketsugu, T.; Hirao, K.; Gordon, M. S. Direct Vibrational Self-Consistent Field Method: Applications to H₂O and H₂CO. *J. Chem. Phys.* **2000**, *113*, 1005–1017.
- (28) Yagi, K.; Hirao, K.; Taketsugu, T.; Schmidt, M. W.; Gordon, M. S. Ab Initio Vibrational State Calculations with a Quartic Force Field: Applications to H₂CO, C₂H₄, CH₃OH, CH₃CCH, and C₆H₆. *J. Chem. Phys.* **2004**, *121*, 1383–1389.
- (29) Yagi, K.; Hirata, S.; Hirao, K. Multiresolution Potential Energy Surfaces for Vibrational State Calculations. *Theor. Chem. Acc.* **2007**, *118*, 681–691.
- (30) Ziegler, B.; Rauhut, G. Efficient generation of sum-of-products representations of high-dimensional potential energy surfaces based on multimode expansions. *J. Chem. Phys.* **2016**, *144*, 114114.
- (31) Yagi, K.; Hirata, S.; Hirao, K. Vibrational Quasi-Degenerate Perturbation Theory: Applications to Fermi Resonance in CO₂, H₂CO, and C₆H₆. *Phys. Chem. Chem. Phys.* **2008**, *10*, 1781–1788.
- (32) Yagi, K.; Otaki, H. Vibrational Quasi-Degenerate Perturbation Theory with Optimized Coordinates: Applications to Ethylene and Trans-1,3-Butadiene. *J. Chem. Phys.* **2014**, *140*, No. 084113.
- (33) Yagi, K. *SINDO 4.0*; 2018.
- (34) Hanson-Heine, M. W. D.; George, M. W.; Besley, N. A. Rapid Anharmonic Vibrational Corrections Derived from Partial Hessian Analysis. *J. Chem. Phys.* **2012**, *136*, 224102.
- (35) Head, J. D. Computation of vibrational frequencies for adsorbates on surfaces. *Int. J. Quantum Chem.* **1997**, *65*, 827–838.
- (36) Besley, N. A.; Metcalf, K. A. Computation of the Amide I Band of Polypeptides and Proteins Using a Partial Hessian Approach. *J. Chem. Phys.* **2007**, *126*, No. 035101.
- (37) Wang, Y.; Bowman, J. M. Towards an Ab Initio Flexible Potential for Water, and Post-Harmonic Quantum Vibrational Analysis of Water Clusters. *Chem. Phys. Lett.* **2010**, *491*, 1–10.
- (38) Liu, H.; Wang, Y.; Bowman, J. M. Quantum Calculations of Intramolecular IR Spectra of Ice Models Using Ab Initio Potential and Dipole Moment Surfaces. *J. Phys. Chem. Lett.* **2012**, *3*, 3671–3676.
- (39) Jacob, C. R.; Reiher, M. Localizing normal modes in large molecules. *J. Chem. Phys.* **2009**, *130*, No. 084106.
- (40) Panek, P. T.; Jacob, C. R. Efficient Calculation of Anharmonic Vibrational Spectra of Large Molecules with Localized Modes. *ChemPhysChem* **2014**, *15*, 3365–3377.
- (41) Panek, P. T.; Jacob, C. R. On the benefits of localized modes in anharmonic vibrational calculations for small molecules. *J. Chem. Phys.* **2016**, *144*, 164111.
- (42) Cheng, X.; Steele, R. P. Efficient anharmonic vibrational spectroscopy for large molecules using local-mode coordinates. *J. Chem. Phys.* **2014**, *141*, 104105.
- (43) Cheng, X.; Talbot, J. J.; Steele, R. P. Tuning vibrational mode localization with frequency windowing. *J. Chem. Phys.* **2016**, *145*, 124112.
- (44) Klinting, E. L.; König, C.; Christiansen, O. Hybrid Optimized and Localized Vibrational Coordinates. *J. Phys. Chem. A* **2015**, *119*, 11007–11021.
- (45) König, C.; Hansen, M. B.; Godtliebsen, I. H.; Christiansen, O. FALCON: A method for flexible adaptation of local coordinates of nuclei. *J. Chem. Phys.* **2016**, *144*, No. 074108.
- (46) Hanson-Heine, M. W. D. Examining the impact of harmonic correlation on vibrational frequencies calculated in localized coordinates. *J. Chem. Phys.* **2015**, *143*, 164104.
- (47) Yagi, K.; Keçeli, M.; Hirata, S. Optimized Coordinates for Anharmonic Vibrational Structure Theories. *J. Chem. Phys.* **2012**, *137*, 204118.
- (48) Yagi, K.; Li, P.-C.; Shirota, K.; Kobayashi, T.; Sugita, Y. A Weight Averaged Approach for Predicting Amide Vibrational Bands of a Sphingomyelin Bilayer. *Phys. Chem. Chem. Phys.* **2015**, *17*, 29113–29123.
- (49) Thomsen, B.; Kawakami, T.; Shigemoto, I.; Sugita, Y.; Yagi, K. Weight-Averaged Anharmonic Vibrational Analysis of Hydration Structures of Polyamide 6. *J. Phys. Chem. B* **2017**, *121*, 6050–6063.
- (50) Yagi, K.; Otaki, H.; Li, P.-C.; Thomsen, B.; Sugita, Y. Weight Averaged Anharmonic Vibrational Calculations: Applications to Polypeptide, Lipid Bilayers, and Polymer Materials. In *Molecular Spectroscopy: A Quantum Chemistry Approach*; Ozaki, Y., Wójcik, M. J., Popp, J., Eds.; Wiley-VCH, in press.
- (51) Shirota, K.; Yagi, K.; Inaba, T.; Li, P.-C.; Sugita, Y.; Kobayashi, T. Detection of sphingomyelin clusters by Raman spectroscopy. *Biophys. J.* **2016**, *111*, 999–1007.
- (52) Warshel, A.; Karplus, M. Calculation of Ground and Excited State Potential Surfaces of Conjugated Molecules. I. Formulation and Parametrization. *J. Am. Chem. Soc.* **1972**, *94*, 5612–5625.
- (53) Warshel, A.; Levitt, M. Theoretical Studies of Enzymic Reactions: Dielectric, Electrostatic and Steric Stabilization of the Carbonium Ion in the Reaction of Lysozyme. *J. Mol. Biol.* **1976**, *103*, 227–249.
- (54) Singh, U. C.; Kollman, P. A. A Combined Ab Initio Quantum Mechanical and Molecular Mechanical Method for Carrying Out Simulations on Complex Molecular Systems: Applications to the CH₃Cl + Cl⁻ Exchange Reaction and Gas Phase Protonation of Polyethers. *J. Comput. Chem.* **1986**, *7*, 718–730.
- (55) Field, M. J.; Bash, P. A.; Karplus, M. A Combined Quantum Mechanical and Molecular Mechanical Potential for Molecular Dynamics Simulations. *J. Comput. Chem.* **1990**, *11*, 700–733.
- (56) Bakowies, D.; Thiel, W. Hybrid Models for Combined Quantum Mechanical and Molecular Mechanical Approaches. *J. Phys. Chem.* **1996**, *100*, 10580–10594.
- (57) Maseras, F.; Morokuma, K. IMOMM: A New Integrated Ab Initio + Molecular Mechanics Geometry Optimization Scheme of Equilibrium Structures and Transition States. *J. Comput. Chem.* **1995**, *16*, 1170–1179.
- (58) Svensson, M.; Humbel, S.; Froese, R. D. J.; Matsubara, T.; Sieber, S.; Morokuma, K. ONIOM: A Multilayered Integrated MO + MM Method for Geometry Optimizations and Single Point Energy Predictions. A Test for Diels-Alder Reactions and Pt(P(t-Bu)₃)₂ + H₂ Oxidative Addition. *J. Phys. Chem.* **1996**, *100*, 19357–19363.
- (59) Eichinger, M.; Tavan, P.; Hutter, J.; Parrinello, M. A Hybrid Method for Solutes in Complex Solvents: Density Functional Theory Combined with Empirical Force Fields. *J. Chem. Phys.* **1999**, *110*, 10452–10467.
- (60) Laio, A.; VandeVondele, J.; Rothlisberger, U. A Hamiltonian Electrostatic Coupling Scheme for Hybrid Car–Parrinello Molecular Dynamics Simulations. *J. Chem. Phys.* **2002**, *116*, 6941.
- (61) Senn, H. M.; Thiel, W. QM/MM Methods for Biomolecular Systems. *Angew. Chem., Int. Ed.* **2009**, *48*, 1198–1229.
- (62) Brunk, E.; Rothlisberger, U. Mixed Quantum Mechanical/Molecular Mechanical Molecular Dynamics Simulations of Biological Systems in Ground and Electronically Excited States. *Chem. Rev.* **2015**, *115*, 6217–6263.
- (63) Cui, Q. Perspective: Quantum Mechanical Methods in Biochemistry and Biophysics. *J. Chem. Phys.* **2016**, *145*, 140901.

- (64) Cui, Q.; Karplus, M. Molecular Properties from Combined QM/MM Methods. I. Analytical Second Derivative and Vibrational Calculations. *J. Chem. Phys.* **2000**, *112*, 1133–1149.
- (65) Nonella, M.; Mathias, G.; Eichinger, M.; Tavan, P. Structures and Vibrational Frequencies of the Quinones in Rb. sphaeroides Derived by a Combined Density Functional/Molecular Mechanics Approach. *J. Phys. Chem. B* **2003**, *107*, 316–322.
- (66) Klähn, M.; Mathias, G.; Kötting, C.; Nonella, M.; Schlitter, J.; Gerwert, K.; Tavan, P. IR Spectra of Phosphate Ions in Aqueous Solution: Predictions of a DFT/MM Approach Compared with Observations. *J. Phys. Chem. A* **2004**, *108*, 6186–6194.
- (67) Babitzki, G.; Mathias, G.; Tavan, P. The Infrared Spectra of the Retinal Chromophore in Bacteriorhodopsin Calculated by a DFT/MM Approach. *J. Phys. Chem. B* **2009**, *113*, 10496–10508.
- (68) Rieff, B.; Bauer, S.; Mathias, G.; Tavan, P. DFT/MM Description of Flavin IR Spectra in BLUF Domains. *J. Phys. Chem. B* **2011**, *115*, 11239–11253.
- (69) Ringer, A. L.; Mackerell, A. D. Calculation of the Vibrational Stark Effect Using a First-Principles Quantum Mechanical/Molecular Mechanical Approach. *J. Phys. Chem. Lett.* **2011**, *2*, 553–556.
- (70) Lyne, P. D.; Hodoscek, M.; Karplus, M. A Hybrid QM-MM Potential Employing Hartree-Fock or Density Functional Methods in the Quantum Region. *J. Phys. Chem. A* **1999**, *103*, 3462–3471.
- (71) Woodcock, H. L.; Hodoscek, M.; Gilbert, A. T. B.; Gill, P. M. W.; Schaefer, H. F.; Brooks, B. R. Interfacing Q-Chem and CHARMM to Perform QM/MM Reaction Path Calculations. *J. Comput. Chem.* **2007**, *28*, 1485–1502.
- (72) Riahi, S.; Rowley, C. N. The CHARMM-TURBOMOLE Interface for Efficient and Accurate QM/MM Molecular Dynamics, Free Energies, and Excited State Properties. *J. Comput. Chem.* **2014**, *35*, 2076–2086.
- (73) Cui, Q.; Elstner, M.; Kaxiras, E.; Frauenheim, T.; Karplus, M. A QM/MM Implementation of the Self-Consistent Charge Density Functional Tight Binding (SCC-DFTB) Method. *J. Phys. Chem. B* **2001**, *105*, 569–585.
- (74) Riccardi, D.; Schaefer, P.; Yang, Y.; Yu, H.; Ghosh, N.; Prat-Resina, X.; König, P.; Li, G.; Xu, D.; Guo, H.; Elstner, M.; Cui, Q. Development of Effective Quantum Mechanical/Molecular Mechanical (QM/MM) Methods for Complex Biological Processes. *J. Phys. Chem. B* **2006**, *110*, 6458–6469.
- (75) Cui, Q.; Elstner, M. Density Functional Tight Binding: Values of Semi-Empirical Methods in an Ab Initio Era. *Phys. Chem. Chem. Phys.* **2014**, *16*, 14368–14377.
- (76) Walker, R. C.; Crowley, M. F.; Case, D. A. The Implementation of a Fast and Accurate QM/MM Potential Method in Amber. *J. Comput. Chem.* **2008**, *29*, 1019–1031.
- (77) Okamoto, T.; Yamada, K.; Koyano, Y.; Asada, T.; Koga, N.; Nagaoka, M. A Minimal Implementation of the AMBER-GAUSSIAN Interface for Ab Initio QM/MM-MD Simulation. *J. Comput. Chem.* **2011**, *32*, 932–942.
- (78) Götz, A. W.; Clark, M. A.; Walker, R. C. An Extensible Interface for QM/MM Molecular Dynamics Simulations with AMBER. *J. Comput. Chem.* **2014**, *35*, 95–108.
- (79) Mendieta-Moreno, J. I.; Walker, R. C.; Lewis, J. P.; Gómez-Puertas, P.; Mendieta, J.; Ortega, J. FIREBALL/AMBER: An Efficient Local-Orbital DFT QM/MM Method for Biomolecular Systems. *J. Chem. Theory Comput.* **2014**, *10*, 2185–2193.
- (80) Isborn, C. M.; Götz, A. W.; Clark, M. A.; Walker, R. C.; Martínez, T. J. Electronic Absorption Spectra from MM and ab Initio QM/MM Molecular Dynamics: Environmental Effects on the Absorption Spectrum of Photoactive Yellow Protein. *J. Chem. Theory Comput.* **2012**, *8*, 5092–5106.
- (81) Phillips, J. C.; Braun, R.; Wang, W.; Gumbart, J.; Tajkhorshid, E.; Villa, E.; Chipot, C.; Skeel, R. D.; Kalé, L.; Schulten, K. Scalable Molecular Dynamics with NAMD. *J. Comput. Chem.* **2005**, *26*, 1781–1802.
- (82) Melo, M. C. R.; Bernardi, R. C.; Rudack, T.; Scheurer, M.; Riplinger, C.; Phillips, J. C.; Maia, J. D. C.; Rocha, G. B.; Ribeiro, J. V.; Stone, J. E.; Neese, F.; Schulten, K.; Luthey-Schulten, Z. NAMD goes quantum: an integrative suite for hybrid simulations. *Nat. Methods* **2018**, *15*, 351–354.
- (83) Field, M. J.; Albe, M.; Bret, C.; Martin, F. P.-d.; Thomas, A. The Dynamo Library for Molecular Simulations Using Hybrid Quantum Mechanical and Molecular Mechanical Potentials. *J. Comput. Chem.* **2000**, *21*, 1088–1100.
- (84) Field, M. J. The pDynamo Program for Molecular Simulations using Hybrid Quantum Chemical and Molecular Mechanical Potentials. *J. Chem. Theory Comput.* **2008**, *4*, 1151–1161.
- (85) Frisch, M. J.; Trucks, G. W.; Schlegel, H. B.; Scuseria, G. E.; Robb, M. A.; Cheeseman, J. R.; Scalmani, G.; Barone, V.; Mennucci, B.; Petersson, G. A.; Nakatsuji, H.; Caricato, M.; Li, X.; Hratchian, H. P.; Izmaylov, A. F.; Bloino, J.; Zheng, G.; Sonnenberg, J. L.; Hada, M.; Ehara, M.; Toyota, K.; Fukuda, R.; Hasegawa, J.; Ishida, M.; Nakajima, T.; Honda, Y.; Kitao, O.; Nakai, H.; Vreven, T.; Montgomery, J. A., Jr.; Peralta, J. E.; Ogliaro, F.; Bearpark, M.; Heyd, J. J.; Brothers, E.; Kudin, K. N.; Staroverov, V. N.; Kobayashi, R.; Normand, J.; Raghavachari, K.; Rendell, A.; Burant, J. C.; Iyengar, S. S.; Tomasi, J.; Cossi, M.; Rega, N.; Millam, J. M.; Klene, M.; Knox, J. E.; Cross, J. B.; Bakken, V.; Adamo, C.; Jaramillo, J.; Gomperts, R.; Stratmann, R. E.; Yazyev, O.; Austin, A. J.; Cammi, R.; Pomelli, C.; Ochterski, J. W.; Martin, R. L.; Morokuma, K.; Zakrzewski, V. G.; Voth, G. A.; Salvador, P.; Dannenberg, J. J.; Dapprich, S.; Daniels, A. D.; Farkas, O.; Foresman, J. B.; Ortiz, J. V.; Cioslowski, J.; Fox, D. J. *Gaussian 09*, revision D.01; Gaussian, Inc.: Wallingford, CT, 2009.
- (86) Shao, Y.; Gan, Z.; Epifanovsky, E.; Gilbert, A. T. B.; Wormit, M.; Kussmann, J.; Lange, A. W.; Behn, A.; Deng, J.; Feng, X.; et al. Advances in molecular quantum chemistry contained in the Q-Chem 4 program package. *Mol. Phys.* **2015**, *113*, 184–215.
- (87) Salahub, D.; Noskov, S.; Lev, B.; Zhang, R.; Ngo, V.; Goursot, A.; Calaminici, P.; Köster, A.; Alvarez-Ibarra, A.; Mejía-Rodríguez, D.; Rezáč, J.; Cailliez, F.; De La Lande, A. QM/MM Calculations with deMon2k. *Molecules* **2015**, *20*, 4780–4812.
- (88) Takano, Y.; Nakata, K.; Yonezawa, Y.; Nakamura, H. Development of Massive Multilevel Molecular Dynamics Simulation Program, Platypus (PLATform for dYnamic Protein Unified Simulation), for the Elucidation of Protein Functions. *J. Comput. Chem.* **2016**, *37*, 1125–1132.
- (89) Metz, S.; Kästner, J.; Sokol, A. A.; Keal, T. W.; Sherwood, P. ChemShell - A Modular Software Package for QM/MM Simulations. *WIREs Comput. Mol. Sci.* **2014**, *4*, 101–110.
- (90) Torras, J.; Roberts, B. P.; Seabra, G. M.; Trickey, S. B. PUPIL: A Software Integration System for Multi-Scale QM/MM-MD Simulations and Its Application to Biomolecular Systems. *Adv. Protein Chem. Struct. Biol.* **2015**, *100*, 1–31.
- (91) Jung, J.; Mori, T.; Kobayashi, C.; Matsunaga, Y.; Yoda, T.; Feig, M.; Sugita, Y. GENESIS: A Hybrid-Parallel and Multi-Scale Molecular Dynamics Simulator with Enhanced Sampling Algorithms for Biomolecular and Cellular Simulations. *WIREs Comput. Mol. Sci.* **2015**, *5*, 310–323.
- (92) Kobayashi, C.; Jung, J.; Matsunaga, Y.; Mori, T.; Ando, T.; Tamura, K.; Kamiya, M.; Sugita, Y. GENESIS 1.1: A Hybrid-Parallel Molecular Dynamics Simulator with Enhanced Sampling Algorithms on Multiple Computational Platforms. *J. Comput. Chem.* **2017**, *38*, 2193–2206.
- (93) Aradi, B.; Hourahine, B.; Frauenheim, T. DFTB+, a sparse matrix-based implementation of the DFTB method. *J. Phys. Chem. A* **2007**, *111*, 5678.
- (94) Best, R. B.; Zhu, X.; Shim, J.; Lopes, P. E. M.; Mittal, J.; Feig, M.; Mackerell, A. D. Optimization of the Additive CHARMM All-Atom Protein Force Field Targeting Improved Sampling of the Backbone ϕ , ψ and Side-Chain χ_1 and χ_2 Dihedral Angles. *J. Chem. Theory Comput.* **2012**, *8*, 3257–3273.
- (95) Zhu, C.; Bryd, R.; Nosedal, J.; Morales, J. L. L-BFGS-B (version 3.0). <http://users.iems.northwestern.edu/nosedal/lbfgsb.html>.
- (96) Byrd, R. H.; Lu, P.; Nocedal, J. A Limited Memory Algorithm for Bound Constrained Optimization. *SIAM J. Sci. Stat. Comp.* **1995**, *16*, 1190–1208.

- (97) Zhu, C.; Byrd, R. H.; Nocedal, J. L-BFGS-B: Algorithm 778: L-BFGS-B, FORTRAN routines for large scale bound constrained optimization. *ACM Transactions on Mathematical Software* **1997**, *23*, 550–560.
- (98) Kästner, J.; Thiel, S.; Senn, H. M.; Sherwood, P.; Thiel, W. Exploiting QM/MM Capabilities in Geometry Optimization: A Microiterative Approach Using Electrostatic Embedding. *J. Chem. Theory Comput.* **2007**, *3*, 1064–1072.
- (99) Eichler, U.; Kölmel, C. M.; Sauer, J. Combining Ab Initio Techniques with Analytical Potential Functions for Structure Predictions of Large Systems: Method and Application to Crystalline Silica Polymorphs. *J. Comput. Chem.* **1997**, *18*, 463–477.
- (100) Besler, B. H.; Merz, K. M., Jr.; Kollman, P. A. Atomic charges derived from semiempirical methods. *J. Comput. Chem.* **1990**, *11*, 431–439.
- (101) Singh, U. C.; Kollman, P. A. An approach to computing electrostatic charges for molecules. *J. Comput. Chem.* **1984**, *5*, 129–145.
- (102) Carter, S.; Culik, S. J.; Bowman, J. M. Vibrational Self-Consistent Field Method for Many-Mode Systems: A New Approach and Application to the Vibrations of CO Adsorbed on Cu (100). *J. Chem. Phys.* **1997**, *107*, 10458–10469.
- (103) König, C.; Christiansen, O. Automatic determination of important mode–mode correlations in many-mode vibrational wave functions. *J. Chem. Phys.* **2015**, *142*, 144115.
- (104) König, C.; Christiansen, O. Linear-scaling generation of potential energy surfaces using a double incremental expansion. *J. Chem. Phys.* **2018**, *145*, No. 064105.
- (105) Madsen, D.; Christiansen, O.; König, C. Anharmonic vibrational spectra from double incremental potential energy and dipole surfaces. *Phys. Chem. Chem. Phys.* **2018**, *20*, 3445–3456.
- (106) Humphrey, W.; Dalke, A.; Schulten, K. VMD: Visual molecular dynamics. *J. Mol. Graphics* **1996**, *14*, 33–38.
- (107) Yu, I.; Mori, T.; Ando, T.; Harada, R.; Jung, J.; Sugita, Y.; Feig, M. Biomolecular Interactions Modulate Macromolecular Structure and Dynamics in Atomistic Model of a Bacterial Cytoplasm. *eLife* **2016**, *5*, 18457.
- (108) Jorgensen, W. L.; Chandrasekhar, J.; Madura, J. D.; Impey, R. W.; Klein, M. L. Comparison of simple potential functions for simulating liquid water. *J. Chem. Phys.* **1983**, *79*, 926–935.
- (109) Ryckaert, J. P.; Ciccotti, G.; Berendsen, H. J. C. Numerical Integration of the Cartesian Equations of Motion of a System with Constraints: Molecular Dynamics of n-Alkanes. *J. Comput. Phys.* **1977**, *23*, 327–341.
- (110) Miyamoto, S.; Kollman, P. A. Settle: An analytical version of the SHAKE and RATTLE algorithm for rigid water models. *J. Comput. Chem.* **1992**, *13*, 952–962.
- (111) Quigley, D.; Probert, M. I. J. Langevin dynamics in constant pressure extended systems. *J. Chem. Phys.* **2004**, *120*, 11432–11441.
- (112) Darden, T.; York, D.; Pedersen, L. Particle mesh Ewald: An Nlog(N) method for Ewald sums in large systems. *J. Chem. Phys.* **1993**, *98*, 10089–10092.
- (113) Essmann, U.; Perera, L.; Berkowitz, M. L.; Darden, T.; Lee, H.; Pedersen, L. G. A smooth particle mesh Ewald method. *J. Chem. Phys.* **1995**, *103*, 8577–8593.
- (114) Becke, A. D. Density-Functional Thermochemistry. III. The Role of Exact Exchange. *J. Chem. Phys.* **1993**, *98*, 5648–5652.
- (115) Lee, C.; Yang, W.; Parr, R. G. Development of the Colle-Salvetti Correlation-Energy Formula into a Functional of the Electron Density. *Phys. Rev. B: Condens. Matter Mater. Phys.* **1988**, *37*, 785–789.
- (116) Dunning, T. H., Jr. Gaussian basis sets for use in correlated molecular calculations. I. The atoms boron through neon and hydrogen. *J. Chem. Phys.* **1989**, *90*, 1007–1023.
- (117) Tosha, T.; Nomura, T.; Nishida, T.; Saeki, N.; Okubayashi, K.; Yamagiwa, R.; Sugahara, M.; Nakane, T.; Yamashita, K.; Hirata, K.; et al. Capturing an initial intermediate during the P450nor enzymatic reaction using time-resolved XFEL crystallography and caged-substrate. *Nat. Commun.* **2017**, *8*, 1585.
- (118) Dennington, R.; Keith, T.; Millam, J. *GaussView, Version 5*; Semichem Inc.: Shawnee Mission, KS, 2009.
- (119) Pettersen, E. F.; Goddard, T. D.; Huang, C. C.; Couch, G. S.; Greenblatt, D. M.; Meng, E. C.; Ferrin, T. E. UCSF Chimera - A visualization system for exploratory research and analysis. *J. Comput. Chem.* **2004**, *25*, 1605–1612.
- (120) Søndergaard, C. R.; Olsson, M. H. M.; Rostkowski, M.; Jensen, J. H. Improved Treatment of Ligands and Coupling Effects in Empirical Calculation and Rationalization of pKa Values. *J. Chem. Theory Comput.* **2011**, *7*, 2284–2295.
- (121) Olsson, M. H. M.; Søndergaard, C. R.; Rostkowski, M.; Jensen, J. H. PROPKA3: Consistent Treatment of Internal and Surface Residues in Empirical pKa Predictions. *J. Chem. Theory Comput.* **2011**, *7*, 525–537.
- (122) Meuwly, M.; Becker, O. M.; Stote, R.; Karplus, M. NO rebinding to myoglobin: a reactive molecular dynamics study. *Biophys. Chem.* **2002**, *98*, 183–207.
- (123) Mishra, S.; Meuwly, M. Nitric Oxide Dynamics in Truncated Hemoglobin: Docking Sites, Migration Pathways, and Vibrational Spectroscopy from Molecular Dynamics Simulations. *Biophys. J.* **2009**, *96*, 2105–2118.
- (124) Feller, S. E.; Zhang, Y.; Pastor, R. W.; Brooks, B. R. Constant pressure molecular dynamics simulation: The Langevin piston method. *J. Chem. Phys.* **1995**, *103*, 4613–4621.
- (125) Martyna, G. J.; Tobias, D. J.; Klein, M. L. Constant pressure molecular dynamics algorithms. *J. Chem. Phys.* **1994**, *101*, 4177–4189.
- (126) Bussi, G.; Donadio, D.; Parrinello, M. Canonical sampling through velocity rescaling. *J. Chem. Phys.* **2007**, *126*, No. 014101.
- (127) Tuckerman, M.; Berne, B. J.; Martyna, G. J. Reversible multiple time scale molecular dynamics. *J. Chem. Phys.* **1992**, *97*, 1990–2001.
- (128) Grimme, S.; Ehrlich, S.; Goerigk, L. Effect of the damping function in dispersion corrected density functional theory. *J. Comput. Chem.* **2011**, *32*, 1456–1465.
- (129) Mardirossian, N.; Head-Gordon, M. ω B97M-V: A combinatorially optimized, range-separated hybrid, meta-GGA density functional with VV10 nonlocal correlation. *J. Chem. Phys.* **2016**, *144*, 214110.
- (130) Rappoport, D.; Furche, F. Property-optimized Gaussian basis sets for molecular response calculations. *J. Chem. Phys.* **2010**, *133*, 134105.
- (131) Weigend, F.; Ahlrichs, R. Balanced basis sets of split valence, triple zeta valence and quadruple zeta valence quality for H to Rn: Design and assessment of accuracy. *Phys. Chem. Chem. Phys.* **2005**, *7*, 3297–3305.
- (132) VandeVondele, J.; Troster, P.; Tavan, P.; Mathias, G. Vibrational Spectra of Phosphate Ions in Aqueous Solution Probed by First-Principles Molecular Dynamics. *J. Phys. Chem. A* **2012**, *116*, 2466–2474.
- (133) Scalmani, G.; Frisch, M. J. Continuous surface charge polarizable continuum models of solvation. I. General formalism. *J. Chem. Phys.* **2010**, *132*, 114110.
- (134) Shiro, Y.; Fujii, M.; Iizuka, T.; Adachi, S.; Tsukamoto, K.; Nakahara, K.; Shoun, H. Spectroscopic and Kinetic Studies on Reaction of Cytochrome P450nor with Nitric Oxide. *J. Biol. Chem.* **1995**, *270*, 1617–1623.
- (135) Obayashi, E.; Tsukamoto, K.; Adachi, S.; Takahashi, S.; Nomura, M.; Iizuka, T.; Shoun, H.; Shiro, Y. Unique Binding of Nitric Oxide to Ferric Nitric Oxide Reductase from *Fusarium oxysporum* Elucidated with Infrared, Resonance Raman, and X-ray Absorption Spectroscopies. *J. Am. Chem. Soc.* **1997**, *119*, 7807–7816.
- (136) Riplinger, C.; Neese, F. The Reaction Mechanism of Cytochrome P450 NO Reductase: A Detailed Quantum Mechanics/Molecular Mechanics Study. *ChemPhysChem* **2011**, *12*, 3192–3203.
- (137) Riplinger, C.; Bill, E.; Daiber, A.; Ullrich, V.; Shoun, H.; Neese, F. New Insights into the Nature of Observable Reaction Intermediates in Cytochrome P450 NO Reductase by Using a

Combination of Spectroscopy and Quantum Mechanics/ Molecular Mechanics Calculations. *Chem. - Eur. J.* **2014**, *20*, 1602–1614.

(138) Paulat, F.; Lehnert, N. Electronic Structure of Ferric Heme Nitrosyl Complexes with Thiolate Coordination. *Inorg. Chem.* **2007**, *46*, 1547–1549.

(139) Praneeth, V. K. K.; Paulat, F.; Berto, T. C.; George, S. D.; Näther, C.; Sulok, C. D.; Lehnert, N. Electronic Structure of Six-Coordinate Iron(III)-Porphyrin NO Adducts: The Elusive Iron(III)-NO(radical) State and Its Influence on the Properties of These Complexes. *J. Am. Chem. Soc.* **2008**, *130*, 15288–15303.

(140) Soldatova, A. V.; Ibrahim, M.; Olson, J. S.; Czernuszewicz, R. S.; Spiro, T. G. New Light on NO Bonding in Fe(III) Heme Proteins from Resonance Raman Spectroscopy and DFT Modeling. *J. Am. Chem. Soc.* **2010**, *132*, 4614–4625.

(141) Spiro, T. G.; Soldatova, A. V.; Balakrishnan, G. CO, NO and O₂ as vibrational probes of heme protein interactions. *Coord. Chem. Rev.* **2013**, *257*, 511–527.